

The AlInP Material System in Heterojunction Bipolar Transistor Technology

by

Ayça Yüksel

Submitted to the Department of Electrical Engineering and Computer Science in partial fulfillment of the requirements for the degrees of

Bachelor of Science

and

Master of Science

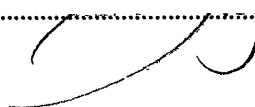
at the

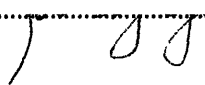
MASSACHUSETTS INSTITUTE OF TECHNOLOGY

January, 1994

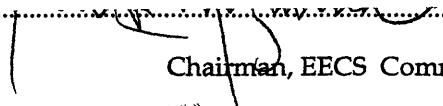
© Ayça Yüksel, 1994. All rights reserved.

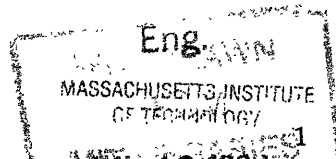
The author hereby grants to MIT permission to reproduce and to distribute copies of this thesis document in whole or in part.

Author.....
 Department of Electrical Engineering and Computer Science
January, 1994

Certified by.....
 Leslie A. Kolodziejski
Associate Professor of Electrical Engineering
Thesis Supervisor

Certified by.....
William U. Liu
Texas Instruments, Inc.
Thesis Supervisor

Accepted by.....
 Frederic R. Morgenthaler
Chairman, EECS Committee on Graduate Students



The AlInP Material System in Heterojunction Bipolar Transistor Technology

by

Ayça Yüksel

Submitted to the Department of Electrical Engineering and Computer Science
on January 31, 1994, in partial fulfillment of the
requirements for the degrees of
Bachelor of Science
and
Master of Science

Abstract

An experimental study was carried out to investigate the use of the AlInP material system in heterojunction bipolar transistor (HBT) technology. This thesis reports the first known d. c. and microwave performance of an AlInP/GaAs HBT. At an operating current density of 4.0×10^4 A/cm², the measured cutoff frequency and the maximum oscillation frequency are 20 GHz and 24.4 GHz, respectively. These high frequency results are respectable considering that the base doping used in the present design is only moderate at a value of 1×10^{19} cm⁻³. In addition, a preliminary passivation experiment and high temperature performance experiment were also conducted on these HBTs.

D. C. performance results of AlInP/GaInP and AlInP/AlGaAs HBTs are presented as well. The current gains were 2 and 4, respectively, for these devices. Tests on GaInP/GaAs and AlGaAs/GaAs HBTs were also conducted for comparison. Current gains of 440 and 70 were reported for these devices. The poor performance of the AlInP/GaInP and AlInP/AlGaAs devices is attributed to a combination of staggered band lineup at the heterointerface and short minority carrier lifetimes in the base region of the transistors.

Thesis Supervisor: Leslie A. Kolodziejski
Title: Associate Professor of Electrical Engineering

Company Thesis Supervisor: William U. Liu
Title: Member of Technical Staff, Texas Instruments, Inc.

Acknowledgments

Any words of thanks are an insufficient expression of my gratitude to the people mentioned in this acknowledgment. I hope that you, and they, will keep this in mind when reading the following section.

First, I want to thank Dr. William Liu for his patience and guidance throughout my time at Texas Instruments. His support and technical knowledge has made this thesis possible.

I am also thankful to Dr. Darrell Hill, whom I consider my "surrogate supervisor". He gave very generously of his time and efforts, especially during my last work period at T. I.

I am grateful to Dr. Dean Collins, who gave me the opportunity to work at T. I. as a part of the VI-A program. This experience has been an invaluable part of my education at MIT.

This work has also benefited greatly from the knowledge and friendships of Terry Session, Jean Ramzel, Wanda Johnson, and Pat Tackett.

In addition, I want to thank Professor Leslie Kolodziejski who guided me in my research and made sure things ran smoothly for me at MIT. Her encouragement and criticisms were a very important contribution, not only to this work but also to my UROP experiences at MIT.

Last, but certainly not least, I must thank Orin Percus for calling me the night before my presentation; Janice Yoo for e-mailing me whenever she could, and Laura Bonner for hunting me down by phone when I moved two offices away. I have collected thirteen years of great experiences and memories between these three people. Their friendship is an inseparable part of who I am, and what I want to be.

A. Y.

January, 1994

Contents

List of Figures	6
List of Tables	9
List of Symbols	10
Introduction	13
1 Background	
1.1 Semiconductor Device Theory.....	14
1.1.1 Homojunction Bipolar Transistors.....	15
1.1.2 Heterojunction Bipolar Transistors.....	19
1.1.2.1 Base Current.....	20
1.2 D. C. Characterization.....	21
1.2.1 Ideality Factor.....	21
1.2.2 Current-Voltage (I-V) Curve for an HBT.....	23
1.2.3 Diode Characteristics.....	24
2 Device Fabrication	
2.1 Design.....	25
2.2 Fabrication.....	28
2.2.1 D. C. Process.....	29
2.2.1.1 Emitter.....	29
2.2.1.2 Base.....	31
2.2.1.3 Collector.....	38
2.2.2 R. F. Process.....	39
2.3 Summary.....	45
3 Device Performance	

3.1	AlInP/GaAs Npn HBT.....	49
3.2	AlInP/GaInP and AlInP/AlGaAs HBTs.....	51
4	Comparison of Different Material Systems	
4.1	GaInP/GaAs and AlGaAs/GaAs HBTs.....	57
4.2	Passivation.....	61
4.3	Temperature Dependence of Current Gain in AlInP/GaAs, AlInP/GaInP, and AlInP/AlGaAs HBTs.....	64
	Conclusions.....	69
	References.....	70

List of Figures

Figure 1.1	The schematic device structures of pnp and npn transistors and their corresponding circuit elements.....	15
Figure 1.2	Equivalent circuit model of an npn transistor.....	15
Figure 1.3	(a) Common-base, (b) Common-collector, and (c) Common-emitter circuit configurations for the bipolar transistor.....	16
Figure 1.4	Simplified band-diagram for a transistor under (a) equilibrium and (b) forward biased conditions.....	16
Figure 1.5	Simplified band diagram for a single heterojunction bipolar transistor.....	19
Figure 1.6	Base current components: I_{br} , I_{re} , I_{cont} and I_{surf} of a typical HBT.....	20
Figure 1.7	Sample Gummel Plot used in measurement of ideality factors of collector and base currents of a transistor.....	22
Figure 1.8	Current-Voltage characteristics of an (a) ideal and (b) non-ideal transistor showing regions of operation and variables of interest.....	23
Figure 2.1	HBT cross-section of an (a) passivated device and (b) non-passivated device. (Note: not drawn to scale).....	26
Figure 2.2	A typical d. c. Npn epitaxial layer structure.....	27
Figure 2.3	(a) Mask pattern of a $100 \times 100 \mu\text{m}^2$ d. c. HBT and (b) SEM micrograph of the actual device.....	29-30
Figure 2.4	Develop photoresist.....	31

Figure 2.5	Evaporate ohmic metal.....	31
Figure 2.6	Completed emitter contact.....	31
Figure 2.7	H ₂ SO ₄ :H ₂ O ₂ :H ₂ O etch to active emitter layer.....	32
Figure 2.8	H ₃ PO ₄ :HCl etch to base layer.....	32
Figure 2.9	SEM images of resultant etches to the base layer of AlInP/GaAs and GaInP/GaAs HBTs.....	33
Figure 2.10	Completed base contact.....	37
Figure 2.11	Develop photoresist.....	38
Figure 2.12	H ₂ SO ₄ :H ₂ O ₂ :H ₂ O etch to subcollector layer.....	39
Figure 2.13	Cross-section of a completed d. c. Npn HBT.....	39
Figure 2.14	SEM image of a two-finger microwave HBT.....	41
Figure 2.15	Schematic picture of a typical two-finger microwave HBT.....	42
Figure 2.16	R. F. processing sequence.....	43
Figure 3.1	I _C -V _{CE} characteristics of an AlInP/GaAs Npn HBT.....	48
Figure 3.2	Gummel Plot of an AlInP/GaAs HBT.....	48
Figure 3.3	Measured current-gain values of a two-finger microwave device having a total emitter area of 2x60 μm ² and a big device having an area of 100x100 μm ²	49
Figure 3.4	High-frequency performance of the 2x60 μm ² AlInP/GaAs device in the common-emitter configuration.....	50
Figure 3.5	Simplified energy-band diagram for an AlInP/AlGaAs/GaAs HBT emphasizing the heterojunction at the base-collector interface.....	52
Figure 3.6	I _C -V _{CE} characteristics and Gummel plots of the processed AlInP/GaInP (a), (b); and AlInP/AlGaAs (c), (d), transistors.....	54
Figure 3.7	Emitter-base band diagram in a typical HBT.....	55
Figure 3.8	Staggered band diagram at the emitter-base junction of an HBT.....	55
Figure 4.1	I _C -V _{CE} plots of (a) AlGaAs/GaAs and (b) GaInP/GaAs HBTs.....	58
Figure 4.2	(a) Gummel plot of GaInP/GaAs HBT and (b) Gummel Plot of an AlGaAs/GaAs HBT.....	59
Figure 4.3	Current gains of all devices: AlInP/GaAs, AlInP/AlGaAs, AlInP/GaInP, GaInP/GaAs, and AlGaAs/GaAs HBTs processed for this investigation.....	60
Figure 4.4	Gummel plot of a passivated 4x20 μm ² AlInP/GaAs device.....	61
Figure 4.5	Current gain versus collector current density for an (a) passivated and (b) unpassivated AlInP/GaAs device.....	62

Figure 4.6	Temperature dependence of current gain in (a) GaInP/GaAs and (b) AlGaAs/GaAs HBTs.....	65
Figure 4.7	Temperature dependence of current gain in (a) AlInP/GaAs, (b) AlInP/AlGaAs, and (c) AlInP/GaInP HBTs.....	67

List of Tables

Table 2.3	Summary of microwave and d. c. device fabrication.....	46
Table 4.1	Transistor parameters measured from the devices fabricated for this investigation.....	60

List of Symbols

α	base transport factor
β	common-emitter, short-circuit, current gain
BV_{ceo}	breakdown voltage
C_{bc}	total base-collector capacitance of device
d	depletion layer width
D_{nb}	hole diffusion coefficient in the base
D_{ne}	electron diffusion coefficient in the emitter
D_{pb}	hole diffusion coefficient in the base
D_{pe}	hole diffusion coefficient in the emitter
E_f	Fermi level under equilibrium conditions
E_f^*	Fermi level under non-equilibrium conditions
E_g	energy gap
E_i	intrinsic Fermi level
ϵ_s	dielectric permittivity
E_v	energy at ceiling of the valence band
f_{max}	maximum oscillation frequency
f_T	cutoff frequency
γ	emitter injection efficiency
G_{max}	maximum available power gain
h_{21}	small-signal current gain
η_b	ideality factor of base current
η_c	ideality factor of collector current
I_b	base current

I_{br}	bulk recombination current in the base region
I_c	collector current
I_{ceo}	common-emitter leakage current
I_{cont}	interface recombination current at the base contact
I_e	emitter current
I_{nc}	collector electron current
I_{ne}	emitter electron current
I_{pb}	base hole current back-injected into the emitter
I_{pe}	hole emitter current
I_{re}	recombination current in the base-emitter depletion region
I_{surf}	surface recombination current in the exposed base region
J_{br}	base bulk recombination current density (A/cm^2)
J_c	collector current density
J_{re}	base-emitter space-charge region recombination current density (A/cm^2)
k	Boltzman constant
K_{surf}	surface recombination current (A/cm)
L_E	emitter length
L_{nb}	electron diffusion length in the base
L_{pe}	hole diffusion length in the emitter
n	electron concentration
n_i	intrinsic electron concentration
n_{ie}	intrinsic carrier concentration in the emitter
N_{ne}	electron concentration in the emitter
N_{pb}	hole concentration in the base
p	hole concentration
p_i	intrinsic hole concentration
q	elementary charge
R_b	base resistance
T	temperature
τ_b	base transit delay
τ_c	collector transit delay
τ_{cr}	collector charging delay
τ_e	emitter charging delay
τ_{eff}	total emitter-collector transit time
τ_{nb}	electron lifetime in the base
V_{bc}	base-collector voltage

V_{be}	emitter-base voltage
$V_{ce(on)}$	offset voltage
W_b	effective base width
W_E	emitter width
W_L	passivation ledge width
X_e	effective emitter thickness
μ_n	electron mobility

Introduction

Recently, GaInP/GaAs structures for Npn heterojunction transistors (HBTs) have received much attention over AlGaAs/GaAs structures, due to the large valence band discontinuity, ΔE_v , of GaInP with respect to GaAs. Similarly, the AlInP/GaAs system is an interesting alternative. AlInP lattice-matched to GaAs is expected to have an even greater ΔE_v than its GaInP counterpart. With a greater ΔE_v in the emitter junction, less base current due to back-injection of holes from the base into the emitter is likely to occur. Therefore, the AlInP/GaAs system appears very promising for Npn HBT applications. This thesis presents the results of the first fabricated AlInP/GaAs Npn HBTs. In this investigation, d. c. current gains of 100 are reported. Microwave testing of the devices yield a cutoff frequency of 20 GHz. The maximum oscillation frequency obtained from the maximum available gain is 24.4 GHz.

The following pages present the discussion of processing and testing of AlInP/GaAs and AlInP/GaInP HBTs. Chapter 1 begins with a description of measurement techniques employed and reviews some pertinent academic background. Chapter 2 discusses the steps followed in the fabrication of the devices, emphasizing the difficulties of etching emitter material and the differences between d. c. and microwave processes. Chapters 3 and 4 present the results obtained for AlInP/GaAs, AlInP/GaInP, AlInP/AlGaAs, AlGaAs/GaAs, and GaInP/GaAs HBTs and compares these five designs for fundamental differences in performance. The last section of this thesis summarizes the conclusions of this work.

Chapter 1

Background

The academic disciplines that are the foundation of much of the work in this thesis are reviewed in the following chapter. Basic semiconductor device physics is used to describe transistor operation and materials characterization. In addition, d. c. measurement techniques used in the preliminary materials and device testing are discussed.

1.1 Semiconductor Device Theory

An introductory course in semiconductor physics that includes concepts of dopants, lattices, carriers, drift, diffusion, recombination-generation, and p-n junctions is helpful in understanding some of the concepts provided here. For reference, see Michael Shur's *Physics of Semiconductor Devices* (1990) or Robert Pierret's *Semiconductor Fundamentals* (1987). An extensive background in transistor structure and operation theory, however, is not assumed. A brief review of the relevant material is presented. For further treatment of this subject matter, see Gerold Neudeck's *The Bipolar Junction Transistor* (1989).

1.1.1 Homojunction Bipolar Transistors

Homojunction Bipolar Transistors (BJTs) are three-terminal devices, fabricated from silicon and related oxides (as well as contact metals and silicides), that are used as amplifiers or logic elements. The schematic device structures of pnp and npn transistors along with their circuit elements are shown in Figure 1.1.

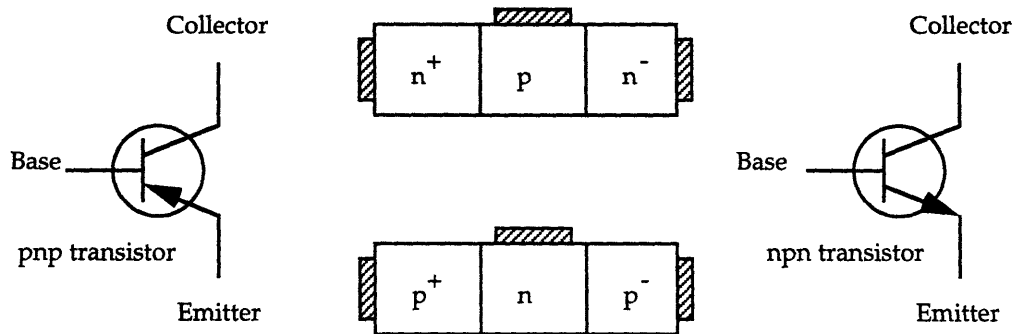


Figure 1.1: The schematic device structures of pnp and npn transistors and their corresponding circuit elements.

Since the work of this thesis focuses primarily on npn transistors, only these will be discussed in further detail. As can be seen from Figure 1.1, a BJT is comprised of two back-to-back p-n junctions. An emitter region and base region form the first p-n junction. The second p-n junction is formed between the base and collector region. Since the base region is typically designed to be much shorter than the diffusion length of minority carriers in the base, these two junctions affect each other and are represented by the presence of controlled current sources in Figure 1.2.

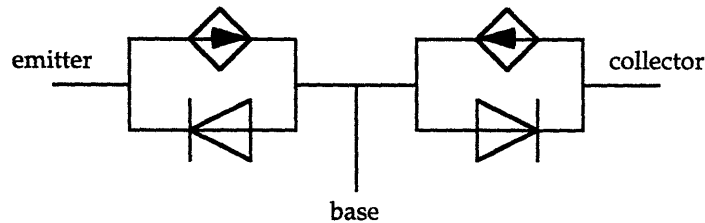


Figure 1.2: Equivalent circuit model of an npn transistor

The minority carrier (electron in this case) diffusion length in the base, L_{nb} , for npn transistors equals $\sqrt{D_{nb}\tau_{nb}}$, where D_{nb} is the electron diffusion coefficient in the p-type base and τ_{nb} is the minority carrier lifetime.

Unlike field-effect transistors (FETs), which can only be modeled as common-source devices, there are three circuit configurations for the bipolar junction transistor. These are the common-base, common-emitter, and common-collector configurations, as shown in Figure 1.3.

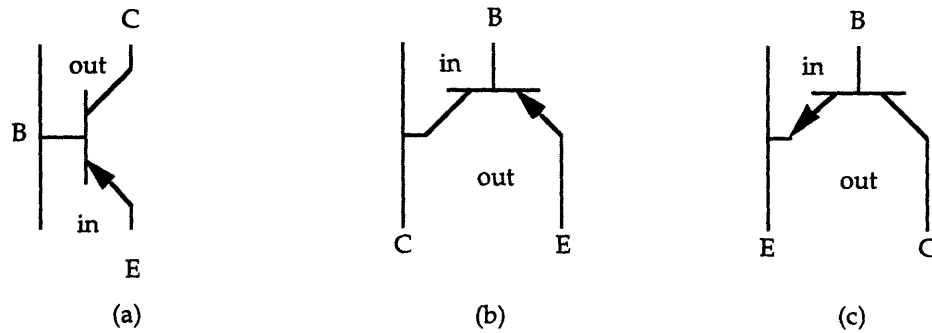
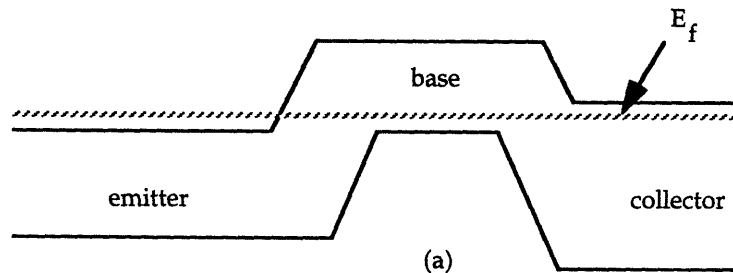


Figure 1.3: (a) Common-base, (b) Common-collector and (c) Common-emitter circuit configurations for the bipolar transistor

Each has a power or current gain associated with it. The most widely employed configuration is that of common-emitter since this provides the narrowest band of frequencies over which the transistor is potentially unstable in high frequency applications. Consequently, the focus of this thesis also falls on the common-emitter configuration of transistors. Therefore, all references to measurements made regarding d. c. characteristics will assume this configuration.

Under normal operating conditions of a BJT (forward active mode), the emitter-base junction (E-B junction) is forward biased, whereas the collector-base junction (C-B junction) is reverse biased. Qualitatively, the effects of biasing can be seen in the band diagram of the BJT. Figure 1.4 compares the band diagram of a transistor under equilibrium (no bias) to that of forward active mode.



(Figure 1.4 continued on next page)

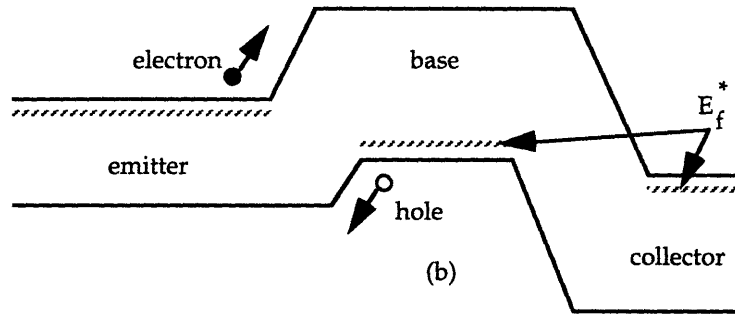


Figure 1.4: Simplified band-diagram for a transistor under (a) equilibrium and (b) forward biased conditions.

The Fermi-Energy or Fermi level, E_f , introduced in Figure 1.4 (a), is computed from carrier concentrations under equilibrium conditions through the following relations:

$$n = n_i \exp\left[\frac{(E_f - E_i)}{kT}\right]$$

and

$$p = p_i \exp\left[\frac{(E_i - E_f)}{kT}\right]$$

Similarly, E_f^* represents the Fermi level computed from carrier concentrations under nonequilibrium conditions. The Fermi energy is referred to in this thesis only in the context of qualitative analysis of band diagrams of processed devices.

As shown in Figure 1.1, the emitter region of a BJT always has the highest doping. The collector region is doped the lowest. The base region has a doping level smaller than that in the emitter region but higher than that in the collector region. Since a transistor is often used as an amplifier or logic element, the reason for such a choice of doping levels is due to the desire for a current gain greater than unity for successful device performance. The desired effect of a large current gain, therefore, is achieved through the implementation of doping profiles and concentrations similar to those qualitatively represented here. Current gain occurs because electrons are injected from the emitter region, through the base, into the collector region, where the voltage drop is large compared with a small forward emitter-base voltage. The details of device design are presented later.

To date, extensive research has been conducted on silicon transistors and current gains of 1000 have been typically reported. However, GaAs, with its superior electrical properties and optical properties, is finding increased usage in a number of applications. Gallium arsenide's

versatility in doping design is also unmatched in Si BJT technology. The resulting impact of the addition of III-V materials on transistor technology is discussed in the next section.

As can be seen from the band diagram of Figure 1.4 (b), there exists another base-emitter current component in BJTs. Composed of holes from the base which are back-injected into the emitter, this current is substantial because both the holes and the electrons experience equal energy barriers at this junction. This is a property of the homojunction. The resultant back-injected current reduces the current gain of the transistor. To minimize this undesirable effect, therefore, the emitter must be more heavily doped than the base. This can be understood from the following equation, which formulates the ratio of desired electron injection current, I_n , from the emitter to the base, over the undesired hole back-injection current, I_p , from the base to the emitter:

$$\frac{I_n}{I_p} = \left[\frac{D_{nb} N_{ne} L_{pe} n_{ie}^2}{D_{pe} N_{pb} W_b n_{ie}^2} \right]$$

where D , N , L , and n_i are diffusion coefficients, doping concentration, diffusion length, and intrinsic carrier concentration, respectively and the subscripts p , n , e , and b stand for holes, electrons, emitter, and base, respectively. W_b is the effective base thickness which is assumed to be less than L_n , the electron diffusion length in the base. As a result of different doping levels, there is greater injection of electrons from the emitter into the base than back-injection of holes from the base into the emitter, allowing for current gain, β , to be greater than unity. Quantitatively, current gain is defined as:

$$\beta = \frac{I_c}{I_b} = \left[\frac{D_{ne} N_{ne} X_e}{D_{pb} N_{pb} W_b} \right] \exp\left(\frac{\Delta E_g}{kT}\right)$$

where ΔE_g is the energy band discontinuity and X_e is the effective emitter thickness. When the emitter doping levels are increased, i.e. N_{ne} is raised, β also increases. However, in practical devices, one must also consider the effects of very high doping levels which lead to changes in material parameters, in particular, to a decrease in the energy gap. Consequently, an exponential ΔE_g dependence is also included in the definition of β for this reason.

Emitter injection efficiency, γ , is another performance parameter used in evaluating device quality. γ measures the ratio of injected electron current to total emitter current:

$$\gamma = \frac{I_{ne}}{I_e} = \frac{I_{ne}}{(I_{ne} + I_{pe})}$$

Note that $\gamma \rightarrow 1$ if $I_{pe} \rightarrow 0$. That is, as the emitter is more heavily doped, I_{pe} becomes a smaller percentage of I_e . For large-gain transistors, γ is made as close to unity as possible.

The design constraint on the emitter of a BJT severely restrains variations on device design in homojunction transistor technology. Specifically, doping and β cannot be varied independently.

1.1.2 Heterojunction Bipolar Transistors

As a result of the limitations that BJT technology imposes on emitter design, heterojunction bipolar transistors (HBTs) have been developed. Fabricated from III-V compounds such as AlAs and GaAs, a typical HBT has an emitter region made of a different material which has a larger bandgap than the rest of the device. This allows for an additional freedom in choosing doping densities of the emitter and base layers. Consequently, with the use of higher base doping, the HBT has lower base resistance and E-B junction capacitance, giving it a significant speed advantage over BJTs. The resulting band diagram is shown in Figure 1.5.

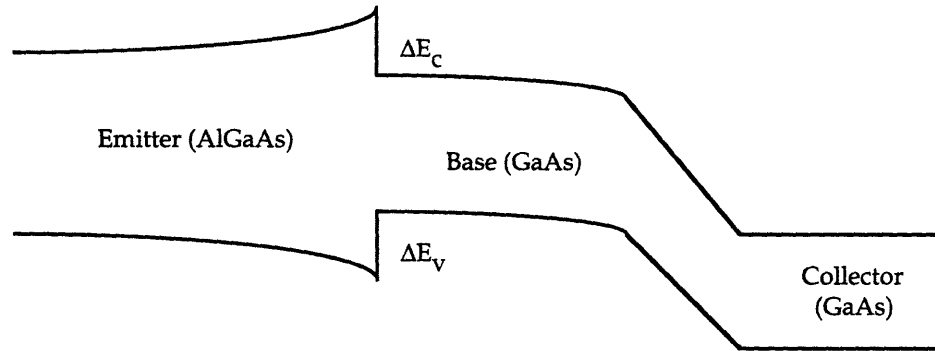


Figure 1.5: Simplified band diagram for a single heterojunction bipolar transistor.

As a result of the abrupt heterojunction, β is also modified to:

$$\beta = \left[\frac{D_n N_{ne} X_e}{D_p N_{pb} W_b} \right] \exp\left(\frac{\Delta E_v}{kT}\right)$$

where ΔE_v is the valence band discontinuity.

1.1.2.1 Base Current

Because of the use of a different emitter material which drastically reduces back-injection of minority carriers from base to emitter, other components of base current emerge. There are four major base current components of the HBTs under consideration: (i) surface recombination current in the exposed base region (I_{surf}); (ii) interface recombination current at the base contact (I_{cont}); (iii) bulk recombination current in the base region (I_{br}); and (iv) recombination current in the base-emitter depletion region (I_{re}). These current components are also illustrated in Figure 1.6.

For the first component, one should note that the surface recombination velocity of GaAs has been found to be relatively high. Since this material is widely used in HBT technology as the base material, it is important to take its surface characteristic into consideration. Because of the high surface recombination velocity on the extrinsic base surface, many minority carriers injected from the emitter recombine with the base majority carriers at this surface. Base contact recombination current is due, again, to a high interface recombination velocity. However, if the base and emitter contact separation is large, then most carriers from the emitter simply cross the base and reach the collector without diffusing to the base contact and recombining there. The third component, I_{br} , exists because of the presence of bulk recombination traps. If the base is excessively thick, most minority carriers recombine in the base before reaching the collector. Finally, I_{re} is E-B space charge (depletion) region recombination current. In the forward-bias E-B junction, a lowered electrostatic potential barrier allows for high concentrations of electrons and holes to diffuse from the neutral base and emitter regions into the depletion region. Because of increased carriers, significant recombination occurs in this region.

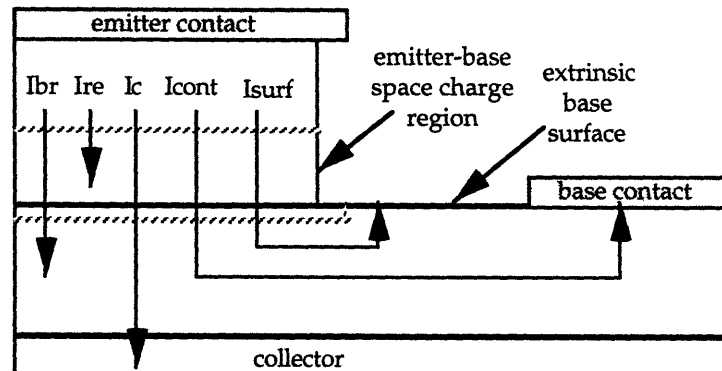


Figure 1.6: Base current components: I_{br} , I_{re} , I_{cont} and I_{surf} , of a typical HBT.

Now, d.c. current gain is limited primarily by these recombination currents:

$$\beta = \frac{I_c}{I_b} = \frac{I_{ne}}{(I_{re} + I_{br} + I_{cont} + I_{surf})}$$

As suggested by the above descriptions, the reduction of most of these components of the base current can be accomplished through device design. HBTs, to date, have been fabricated with AlGaAs/GaAs and GaInP/GaAs as emitter/base material. This thesis also investigates AlInP/GaAs and AlInP/GaInP as possible additions to the combinations of III-V materials suitable for semiconductor applications. The methods of device performance evaluation are discussed in the next section.

1.2 D. C. Characterization

In the d. c. characterization of bipolar transistors, one of the most important parameters is the d. c. current gain, β . Therefore, the analysis of various factors affecting β is the primary concern of this paper. The tools used in this analysis; current-voltage curves, Gummel plots, and p-n junction diode characteristics, as well as the variables under question: β , leakage current, and the ideality factor, will be summarized here.

1.2.1 Ideality Factor

I_{bulk} and I_{surf} , as noted before, result from intrinsic bulk and extrinsic surface recombination, respectively. It is important to determine which of these components dominates the base current of a transistor in order to optimize the device's performance. In general, knowledge of the ideality factor of various current components as a function of base-emitter voltage, V_{be} , and temperature enables one to better understand and interpret the experimental results.

The ideality factor, η , of a current can be derived from the current-voltage relationship of the transistor. Quantitatively, η_c and η_b are ideality factors of the collector and base currents, respectively, and are related to the currents as shown in the following equations:

$$\begin{aligned} \eta_c: \quad I_c &= I_{co} \exp\left(\frac{qV_{be}}{\eta_c kT}\right) \\ &\text{and} \\ \eta_b: \quad I_b &= I_{bo} \exp\left(\frac{qV_{be}}{\eta_b kT}\right) \end{aligned}$$

Experimental results have shown that $\eta_c \sim 1$ for a graded¹ E-B junction HBT, ~ 1.1 for an abrupt² junction HBT, and ~ 1.3 for a junction with InP material.³ Experimental and theoretical evidence also show that $\eta_b = 1$ for I_{bulk} , 2 for I_{re} and 1 for I_{surf} .^{4,5} The ideality factor can readily be deduced from I_c and I_b versus V_{be} curves showing collector and base current with respect to E-B junction bias (V_{be}). A sample plot is shown in Figure 1.7. This plot is called a Gummel plot and the areas of linearity of the currents mark the range of V_{be} bias for which the ideality factor is of concern. The base-collector bias, V_{bc} , is kept at zero for these measurements.

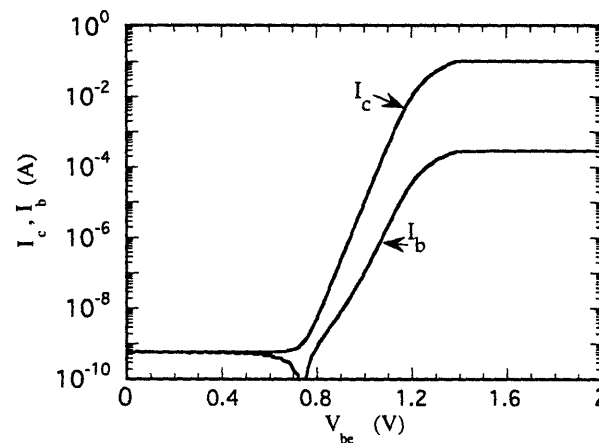


Figure 1.7: Sample Gummel Plot used in measurement of ideality factors of collector and base currents of a transistor.

¹ refers to devices with a gradual variation of aluminum composition over the base-emitter junction (typically AlGaAs emitter and GaAs base).

² refers to devices where the aluminum composition in the entire emitter (typically AlGaAs) remains unchanged.

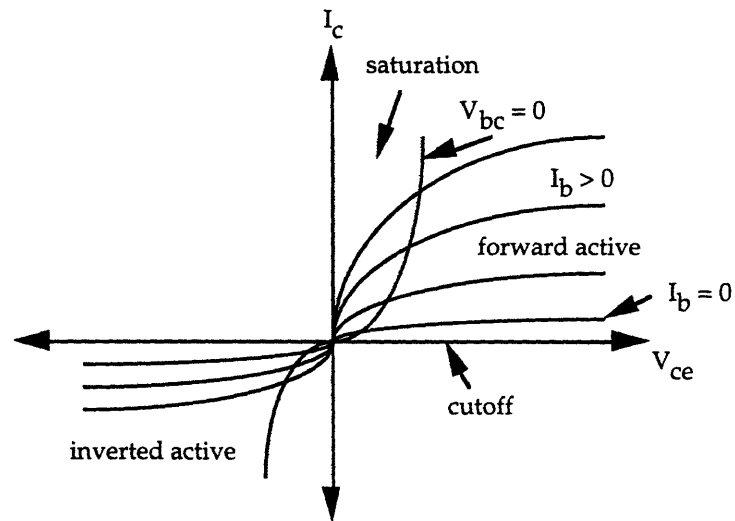
³ "Current Transport Mechanism in GaInP/GaAs Heterojunction Bipolar Transistors," W. Liu, S. Fan, T. Kim, E. Beam, D. Davito. *IEEE Transactions on Electron Devices*, vol. 40, no. 8. August 1993.

⁴ "Diode Ideality Factor for Surface Recombination Current in AlGaAs/GaAs Heterojunction Bipolar Transistors," W. Liu, J. Harris, Jr. *IEEE Transactions on Electron Devices*, vol. 39, no. 12. December 1992.

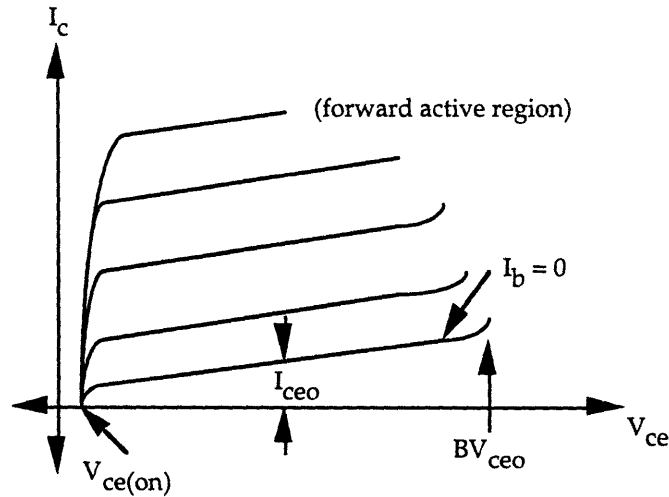
⁵ "Extrinsic Base Surface Passivation in GaInP/GaAs Heterojunction Bipolar Transistors," W. Liu, E. Beam, T. Henderson, S. Fan, *IEEE Electron Device Letters*, vol. 14, no. 6. June 1993.

1.2.2 Current-Voltage (I-V) curve for an HBT

This section discusses the current-voltage (I-V) characteristics of a typical HBT. Figure 8 compares ideal and non-ideal I-V curves. As can be seen from these graphs, there are four regions of operation: cutoff, saturation, forward active, and inverted active. When compared to the ideal I-V curve of Figure 1.8 (a), the non-ideal curve (Figure 1.8 (b)) shows several interesting discrepancies.



(a)



(b)

Figure 1.8: Current-Voltage characteristics of an (a) ideal and (b) nonideal transistor showing regions of operation and variables of interest.

First, the slope of the forward-active common-emitter non-ideal I-V curve is due to the generation current produced in the C-B depletion region. Electrons and holes are generated, each contributing to an increase in collector current (I_C) as the C-B depletion region increases under increased reverse bias. However, the largest increase is a result of the generated holes drifting into the base, where they become majority carriers. In the case of a microwave device, leakage current due to implantation damage is also of concern. The generated holes in the base-collector depletion region add directly to the back-injected holes at the E-B junction which forces a much larger increase in the injected electrons from the emitter which, in turn, diffuse to the collector junction and increase I_C significantly. At $I_B = 0$, this observed phenomenon is referred to as the collector-emitter leakage current, I_{CE0} . Leakage current is an unwanted effect since it causes a steady increase of current gain over the measured range of collector current. Ideally, one wants a constant current gain for a given range of I_C for reasons of reliability and reproducibility of transistor performance.

The common-emitter avalanching characteristic is also illustrated in Figure 1.8 (b) and is characterized by the second variable of interest, the breakdown voltage of collector-emitter, BV_{CE0} . This breakdown voltage is defined with the base open-circuited.

1.2.3 Diode characteristics

Lastly, each of the junctions, E-B and C-B, are p-n junction diodes. As discussed previously, measurement of the I-V characteristics of the diodes can give valuable information on leakage current and turn-on voltage of the transistor. Typically, turn-on voltage for the emitter-base heterojunction is 1.1 ~ 1.2 V. The collector-base homojunction turns on at ~ 0.7 - 0.9 V. The difference in turn-on of these two junctions results in an offset voltage of the same magnitude for the transistor. The offset voltage, $V_{ce(on)}$ is, in effect, the point at which the transistor begins to operate.

Chapter 2

Device Fabrication

The purpose of this chapter is to detail the methods of design and fabrication used in making the devices under investigation. The section on design gives some broad guidelines to consider when deciding upon doping densities and layer thicknesses. The section titled "Fabrication" describes the steps used in the actual processing of the transistors.

2.1 Design

In order to facilitate the methods of comparison, we adopt the same structures for AlInP/GaAs and AlInP/GaInP HBTs that are used in GaInP/GaAs and AlGaAs/GaAs material systems. The chosen doping levels of emitter, base, and collector, minimize bulk resistances while still yielding respectable values of current gain. The base region is designed to be much shorter than the diffusion length of the minority carriers in the base, thereby minimizing loss of carriers due to recombination. One of the most important design considerations is in the reduction of the base current components. Given the definitions of these components (section

1.2.1), one can make certain preferences in the mask design or device structure. For example, I_{cont} is reduced if the base-emitter contact separation is large (much longer than the base thickness). Then, most carriers from the emitter simply cross the base and reach the collector without diffusing to the base contact and recombining there. I_{br} is also reduced if the base is designed to be thin so that a negligible number of carriers recombine in the base before reaching the collector. Finally, the extrinsic base surface recombination current is reduced through surface passivation with a depleted ledge composed of the active emitter material. Figure 2.1 compares an HBT structure with a passivation ledge (a) to one which has not been passivated (b).

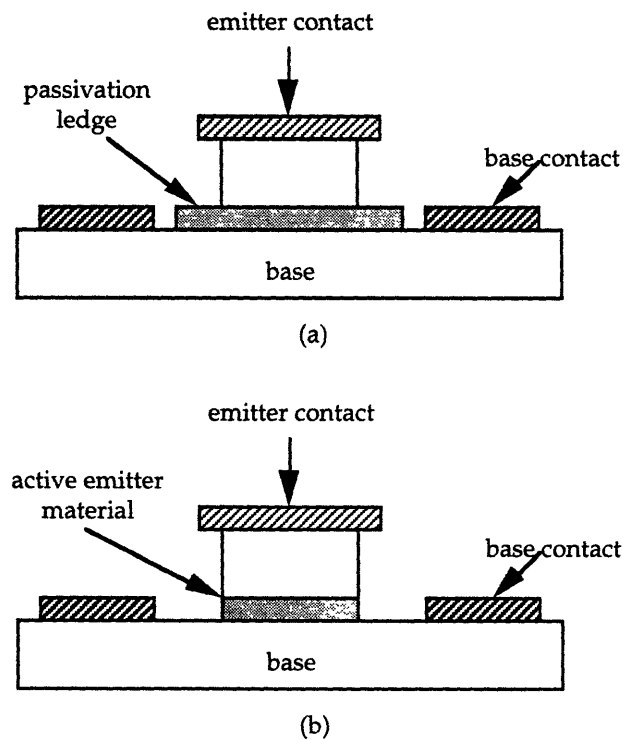


Figure 2.1: HBT cross-section of (a) a passivated device and (b) non-passivated device. Shaded region indicates that the emitter is composed of different material than either the cap or base regions. (Note: not drawn to scale)

The passivated device has a ledge which is depleted due to the combination of the surface depletion region and the p-n junction depletion region. As a result, this depleted ledge reduces carriers at the surface which, otherwise, tend to recombine and, therefore, increase I_b . Optimal thicknesses of the ledges are dependent on the material used and have been experimentally

determined to be between 700-1000 Å for AlGaAs and GaInP material.^{3,6,7} Emitter, base, and collector doping levels are also determined by considering material resistivity. For example, base bulk recombination current increases with base doping due to the decrease in the minority carrier lifetime of the material as a result of recombination. For high frequency applications, however, a high base doping level is desired, as discussed in Chapter 3. Therefore, a compromise must be made on the base doping in order to optimize transistor performance.

The basic structure of a device used in this investigation is illustrated in Figure 2.2.

<u>doping (1/cm³)</u>		<u>layer</u>
5x10 ¹⁸	2000 Å n ⁺ GaAs	cap
5x10 ¹⁷	1000 Å n AlInP	emitter
1x10 ¹⁹	1000 Å p ⁺ GaAs	base
2x10 ¹⁶	5000 Å n ⁻ GaAs	collector
3x10 ¹⁸	1 μm n ⁺ GaAs	subcollector
	substrate (GaAs)	

Figure 2.2: A typical d. c. Npn epitaxial layer structure

Cap and subcollector layers are doped higher to reduce contact resistance. In this investigation, the active emitter layer was also composed of AlGaAs or GaInP material. The base and collector layers are typically GaAs, although some devices with GaInP or AlGaAs base, and GaInP collector layers have also been processed for this study. For ease of comparison, the thicknesses and doping levels used are identical across all of the material systems used: AlGaAs/GaAs, GaInP/GaAs, AlInP/GaInP, AlInP/AlGaAs, and AlInP/GaAs. In addition, the device structure

⁶ *Pnp Heterojunction Bipolar Transistors in AlGaAs/InGaAs/GaAs*, D. Hill, Ph.D. Dissertation, Stanford University, Stanford, CA, pp. 74-87. June 1990.

⁷ "Extrinsic Base Surface Recombination Current in GaInP/GaAs Heterojunction Bipolar Transistors with near-Unity Ideality Factor", W. Liu, *Jpn. J. Appl. Phys.* vol 32, 1993, pp. 713-715.

employed here has been used extensively in the GaInP/GaAs and AlGaAs/GaAs material systems, yielding well-established and previously published results.

The HBT material was grown with metalorganic molecular beam epitaxy (MOMBE). Elemental Be and Sn were used for p and n type dopant sources, respectively. The Al source for AlInP was elemental aluminum evaporated from a conventional effusion cell. The AlInP layer was grown at 500° C at a growth rate of ~ 0.9 $\mu\text{m/hr}$, with a V:III ratio of less than five. In addition, elemental Ga and In sources were used for the GaAs, AlGaAs, and GaInP layers.⁸

The principal test of material quality was device performance using the MOMBE grown layers of AlInP, GaInP, AlGaAs, and GaAs. The obtained results for the AlInP devices were compared to published reports on better known material systems of GaInP and GaAs. Consequently, the doping densities and layer thicknesses used in this investigation were borrowed from previously published work of GaInP and GaAs device structures in order to facilitate comparisons between material systems. In the future, however, a thorough investigation of the AlInP material system requires specific tests to assess the quality of the epilayers, such as Hall measurements to determine mobility, photoluminescence studies on lattice mismatch at the interface, X-ray diffraction measurements to observe variations in lattice constant versus film thickness, and double crystal X-ray diffraction rocking curves to study the effect of various parameters involved in film growth on the crystal structure of the epitaxial layers. Transmission electron microscopy (TEM), scanning electron microscopy (SEM), and high-resolution electron microscopy (HREM) can also be used to study the effects of lattice-mismatch and the subsequent dislocations found at the interface.

2.2 Fabrication

The device fabrication techniques described here are primarily those of the transistors made for d. c. characterization. Because one AlInP/GaAs wafer was also processed for high-frequency testing, however, this technique will also be discussed briefly.

⁸ The Use of Tertiarybutylphosphine and Tertiarybutylarsine for the Metalorganic Molecular Beam Epitaxy of the InGaAs/InP and InGaP/GaAs Material Systems," E. A. Beam III, T. S. Henderson, and J. Y. Yang, *Journal of Crystal Growth*, vol 116, 1992, pp. 436-446.

2.2.1 D. C. Process

The mask design used (a) and a scanning electron microscope (SEM) micrograph (b) of the actual device are shown in Figure 2.3.

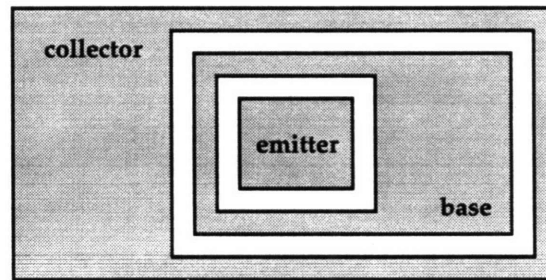
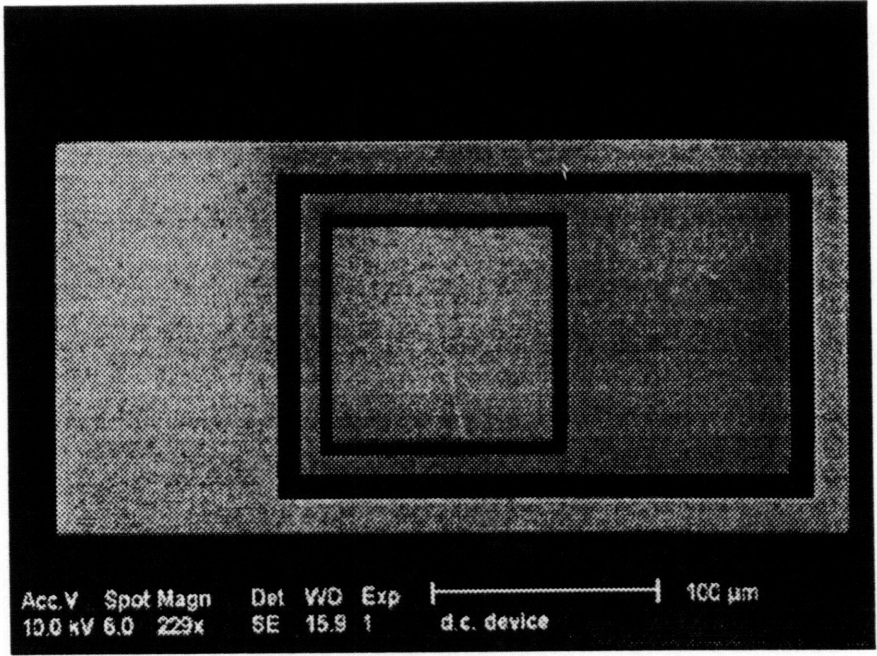


Figure 2.3: (a) Mask pattern of a $100 \times 100 \mu\text{m}^2$ d. c. HBT. The shaded region indicates areas with metal contacts.

This d. c. device is used in the preliminary testing of the material quality. The d. c. current gain, β , measured from the device as well as its current-voltage characteristics, can give great insight into the appropriateness of a given material system for use in transistor technology. The steps followed in processing each layer are given in the following sections.

2.2.1.1 Emitter

The emitter layer contact deposition begins with a solvent cleaning of the surface to remove residual dirt and grease. Next, photoresist is applied using a spin-on technique and exposed with the emitter mask pattern. In this case, photoresist was spun on the wafer at a rate of 3725 rpm for 20 seconds. The development time ranged from three to four minutes depending on exposure intensity used. Figure 2.4 illustrates the resultant profile after the photoresist is developed.



12190

Figure 2.3: (b) SEM micrograph of the actual HBT d. c. device

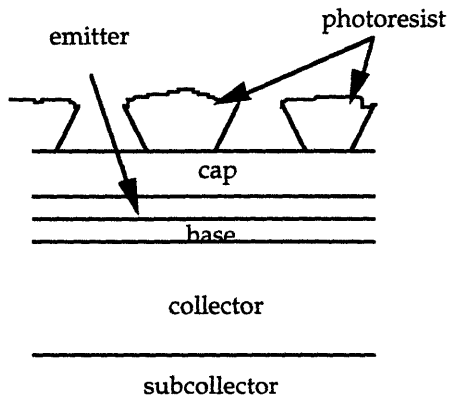


Figure 2.4 Develop photoresist

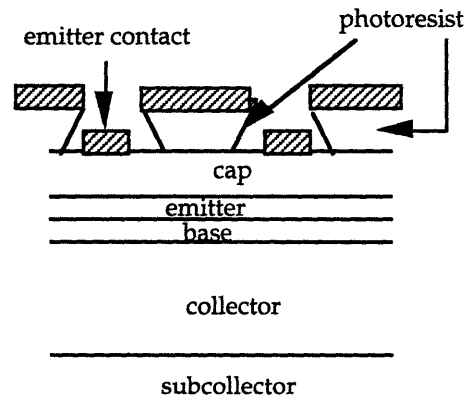


Figure 2.5: Evaporate ohmic metal

Next, AuGe/Ni/Au ohmic contacts are deposited on the surface (Figure 2.5); and the resist is lifted off with acetone. (Fig 2.6). Once the emitter contacts are evaporated, the wafer is ready for base layer process.

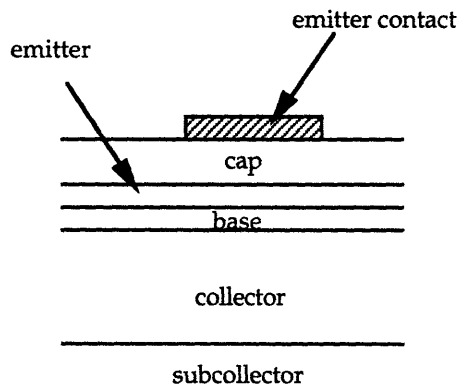


Figure 2.6: Completed emitter contact

2.2.1.2 Base

The most difficult step involved in forming the base contact is the etch to the base layer. The emitter contacts are used as a natural mask pattern to wet-etch regions other than the emitter

mesa down to the base layer. Using previously published reports^{9, 10, 11, 12} on etchants as a guideline, the cap layer of GaAs is etched in a solution of $H_2SO_4:H_2O_2:H_2O$ to expose the active emitter material, as shown in Figure 2.7.

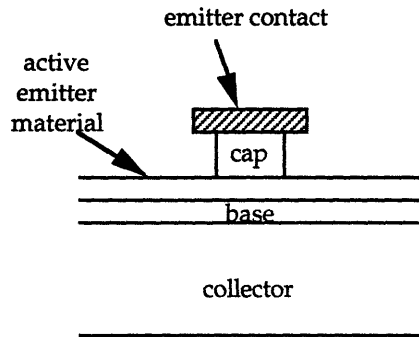


Figure 2.7: $H_2SO_4:H_2O_2:H_2O$ etch to active emitter layer

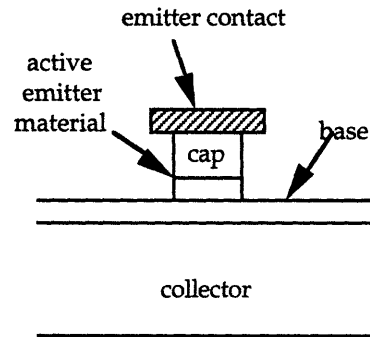


Figure 2.8 $H_3PO_4:HCl$ etch to base layer.

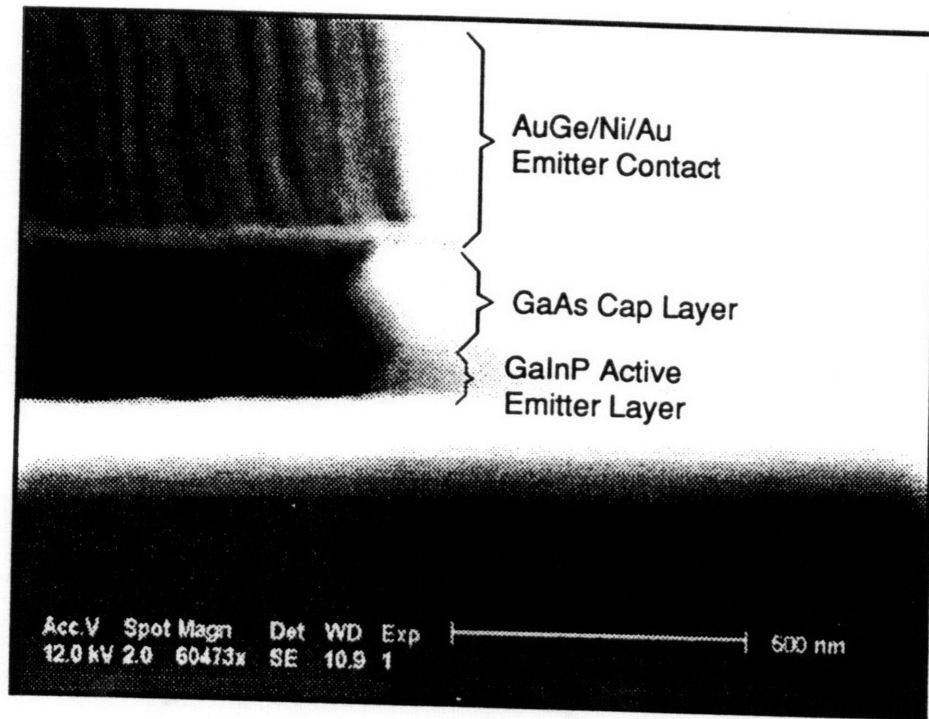
Next, the active emitter material, AlInP, is etched. At this point, a dilute solution containing $H_3PO_4 : HCl$ or $H_2O : HCl$ is used for AlInP. HCl also attacks GaInP, however, and if the emitter material is GaInP, a higher concentration of HCl in solution should be used to properly etch this layer. A 3:1, $H_3PO_4 : HCl$ solution was used for GaInP, and a 30:1 $H_3PO_4:HCl$ solution was used for AlInP in this investigation. In the case of AlGaAs emitter material, an etchant containing H_2SO_4 , H_2O_2 , and H_2O is used to etch through the emitter layer (Fig. 2.8). SEM micrographs of resultant etches to the base layer of AlInP/GaAs and GaInP/GaAs HBTs are shown in Fig. 2.9.

⁹ "Selective Wet Etching of GaInP, GaAs, & InP in Solutions of HCl, CH_3COOH , and H_2O_2 ," J. R. Flemish and K. A. Jones, *J. Electrochem.Soc.*, vol. 140, no. 3. March 1993.

¹⁰ "Wet and Dry Etching Characteristics of AlInP," J. R. Lothian, J. M. Kuo, W. S. Hobson, E. Lane, F. Ren, and S. J. Pearton, *J. Vac. Sci. Technol, B* 10(3). May/June 1992.

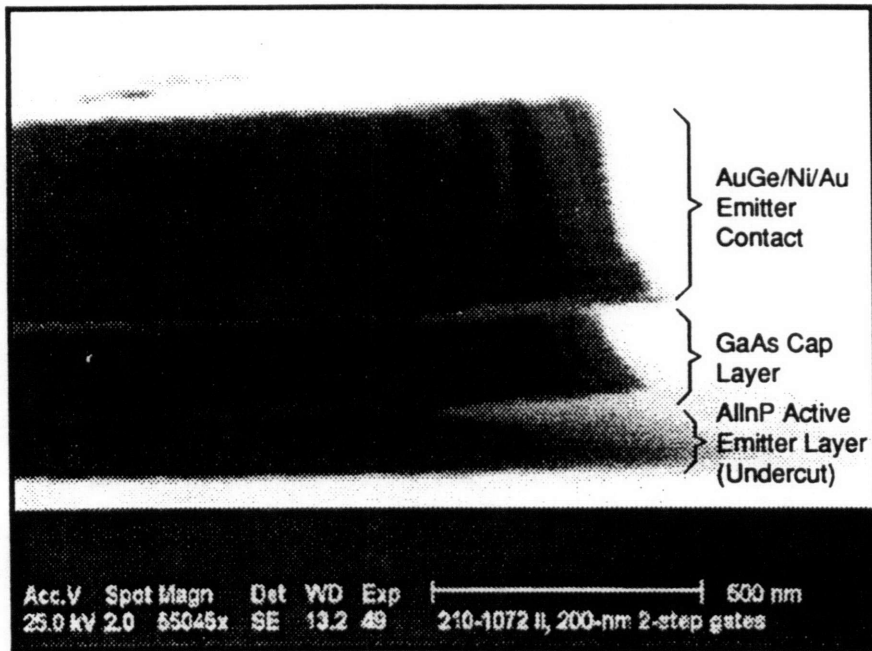
¹¹ "Etch Rates and Selectivities of Citric Acid / Hydrogen Peroxide on GaAs, AlGaAs, InGaAs, InAlAs, and InP," G. C. DeSalvo, W. F. Tseng, J. Comas, *J. Electrochem. Soc.*, vol. 139, no.3. March 1992.

¹² "Plasma and Wet Chemical Etching of InGaP," J. R. Lothian, J. M. Kuo, F. Ren, S. J. Pearton, *Journal of Electronic Materials*, vol. 21, no.4. 1992.



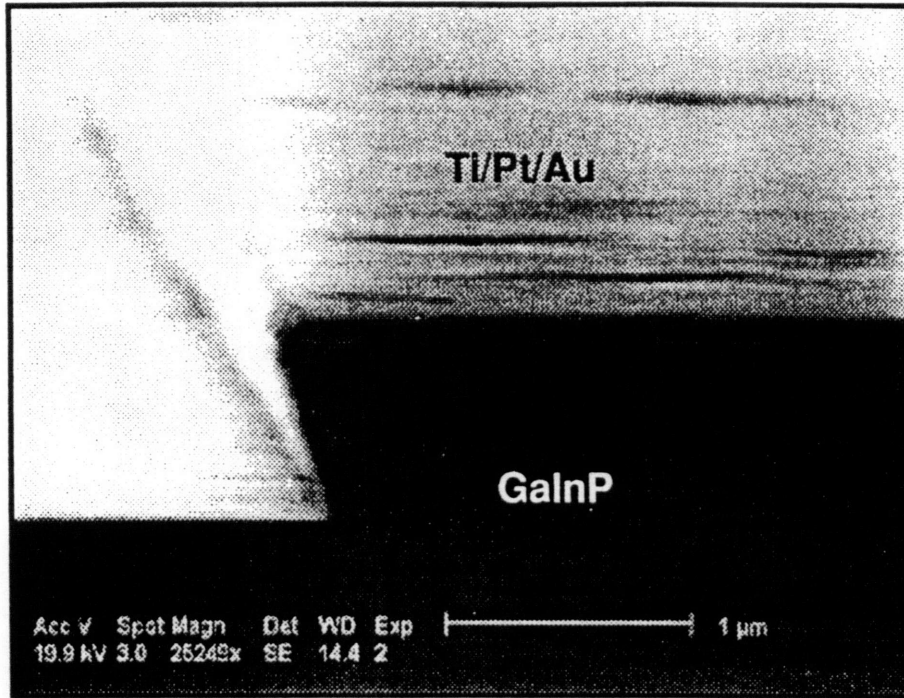
12193

Figure 2.9 (a): SEM micrograph of an emitter contact and etch to the base layer of a GaInP/GaAs HBT



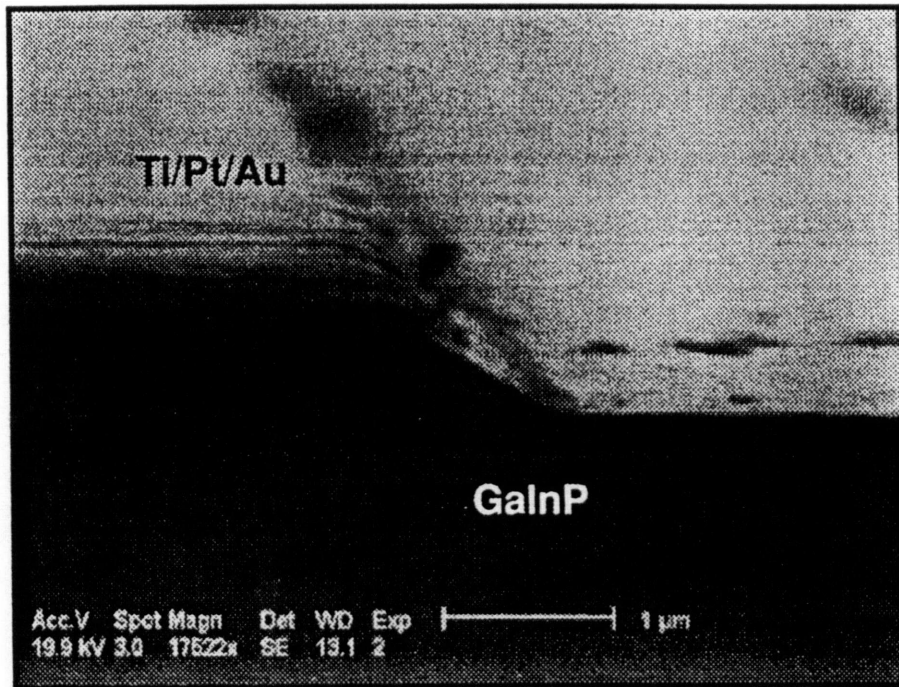
12191

Figure 2.9 (b): SEM micrograph of the emitter contact and etch to the base layer of an AlInP/GaAs HBT



12791

Figure 2.9 (c): SEM image of GaInP profile etched in $\text{H}_3\text{PO}_4:\text{HCl}$ and cleaved along $[0\bar{1}1]$ crystal orientation. (Note: No cap layer of GaAs for this sample)



12792

Figure 2.9 (d): SEM image of a GaInP profile etched in $\text{H}_3\text{PO}_4:\text{HCl}$ and cleaved along [011] crystal orientation. (Note: No cap layer of GaAs for this sample)

The SEM micrographs also emphasize the importance of contact pattern orientation with respect to the wafer since etch profiles change drastically for different planes of crystal geometry of the material in question.

In cases where the emitter material is either GaInP or AlInP, the process is described as a selective etch since the acids used to etch GaInP and AlInP stop at the GaAs base layer. This characteristic of the etchant is particularly useful if one has to etch to a very thin base layer and accidentally etching through the base becomes a concern. (Care must still be taken to time the etch properly in order to prevent excessive undercut of the emitter contacts.) This, however, is not the case for AlGaAs/GaAs HBTs where $H_2SO_4:H_2O_2:H_2O$ is used to etch through both the AlGaAs emitter layer and the GaAs base layer.

After the base contact etch, the base contact region is defined with the base mask pattern by application of the resist using a spinner, exposure, and development. Finally, Ti/Pt/Au contacts are evaporated on the surface. The resist is then lifted off. The result is illustrated in Figure 2.10.

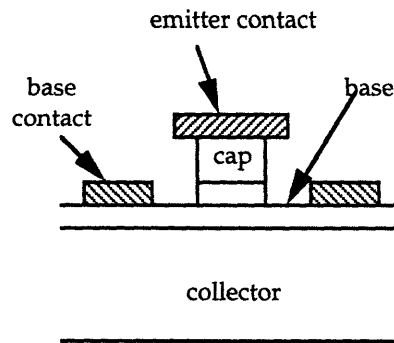


Figure 2.10: Completed base contact

2.2.1.3 Collector

Since the collector is of the same material as the base, and stopping the etch right at the subcollector layer is not an issue, collector contact lithography is a far simpler process. First, resist is applied using a spin-on technique, exposed, and developed. Then, the GaAs (or GaInP, depending on base material used) is etched through the base and the collector layers to the subcollector. In this case, since the collector contact covers the entire periphery of the emitter and base patterns (Figure 2.3), an etch with the resist pattern results in device isolation. Figure 2.11 shows a cross-section of the device after resist development.

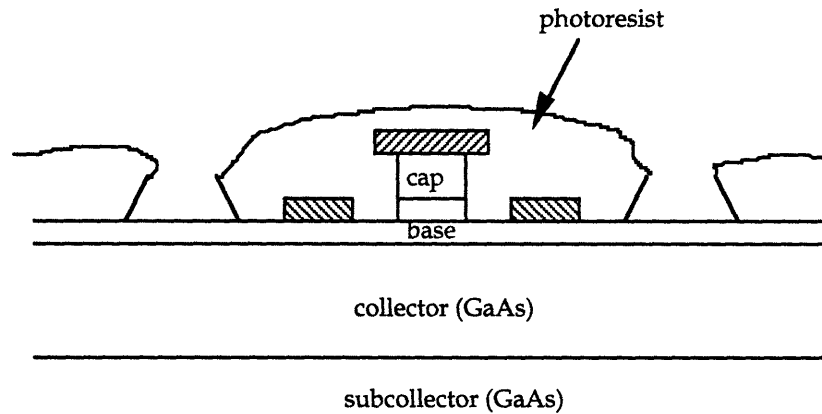


Figure 2.11: Develop photoresist

The etch rate is controlled through timing and concentration of solution and the etch depth is monitored through alpha-step measurements and probing of the surface breakdown voltage. The material is etched until the subcollector is reached because the subcollector is doped with a higher concentration than the collector, thereby reducing contact resistance. (Figure 2.12)

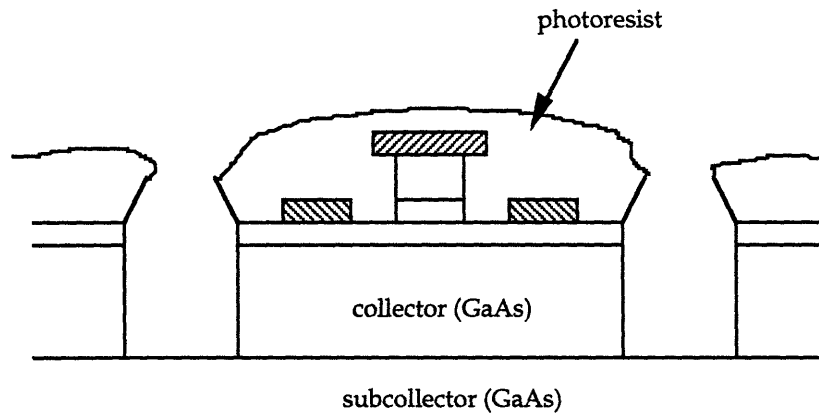


Figure 2.12: $\text{H}_2\text{SO}_4:\text{H}_2\text{O}_2:\text{H}_2\text{O}$ etch to subcollector layer

Finally, AuGe/Ni/Au contacts are evaporated and the resist is lifted off. As a final step in the process, the completed device is alloyed at 430°C in order to reduce contact resistances. A cross-section of a finished d. c. heterojunction bipolar transistor is shown in Figure 2.13.

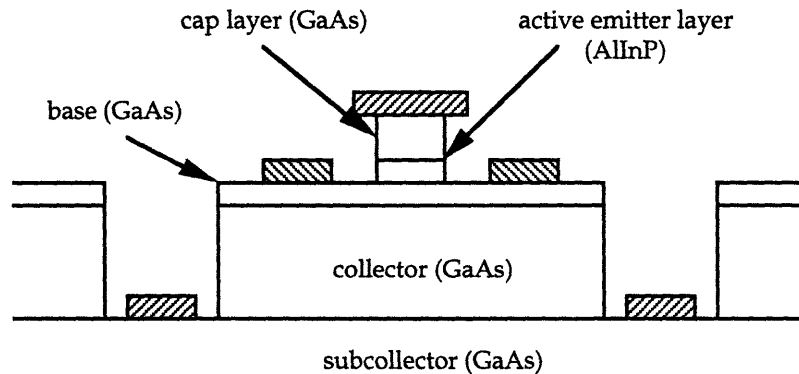


Figure 2.13: Cross-section of a completed d.c. Npn HBT

2.2.2 R. F. Process

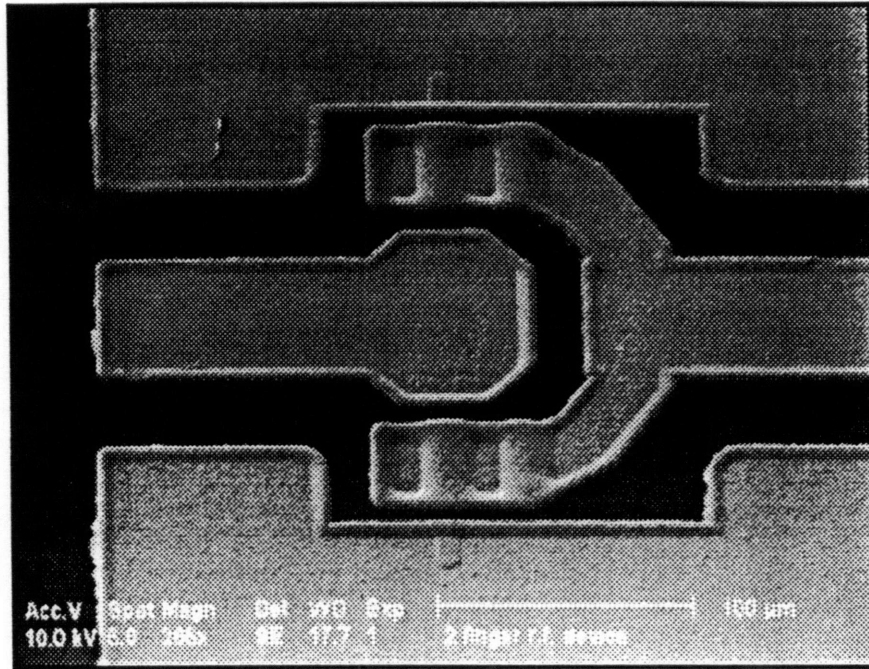
The r. f. process differs from the d. c. process both in mask pattern used and method of isolation of devices. Importance is also given to the quality of contacts as one strives to minimize parasitic effects which tend to slow down device performance. Air bridges are used to connect collectors in multiple-finger devices.

Figure 2.14 shows an SEM image of a finished HBT. A schematic in Figure 2.15 of an microwave device helps to clarify the various parts of the transistor.

The first difference between r. f. and d. c. devices is in the mask pattern. For r. f. devices, the collector contact does not surround the emitter and base contacts. Therefore, other means must be employed in order to achieve device isolation. Ion implantation techniques are used for this purpose. Ions having high kinetic energies, are implanted into the surface and serve to disrupt the ordered lattice of the epitaxial layers, thereby creating a nonconducting barrier between devices. The consequences of this implantation, however, result in difficulties in etching the disordered surface areas, particularly in the GaInP active emitter layer.

Contact annealing is an additional step in the emitter process sequence of microwave devices. Heating contacts to temperatures above 200° C after evaporation and liftoff improves the semiconductor and contact interface by increasing the diffusion of GaAs from the cap layer into the ohmic contact, thereby facilitating conduction across this interface.

Passivation of transistors is also a design consideration in small, r. f., devices. Specifically, extrinsic base surface recombination current is proportional to the length of the emitter periphery. For microwave devices in specific, the emitter width is 2 μm or less, which is drastically smaller than the emitter length ($\sim 30 \mu\text{m}$). Therefore, in unpassivated devices where the extrinsic base surface recombination current is significant, the current gain decreases as the emitter area decreases. A study of current gain in these devices must take this design variable into consideration.



12194

Figure 2.14: SEM image of a two-finger microwave HBT

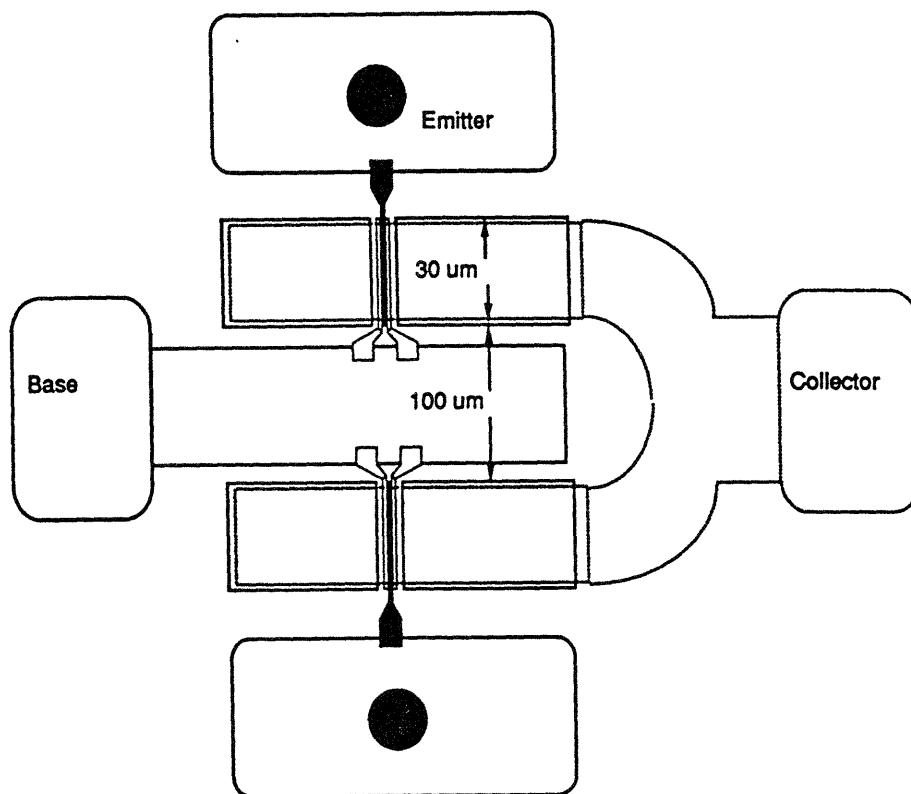
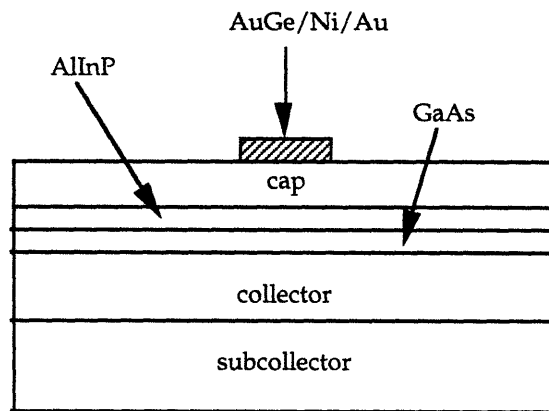


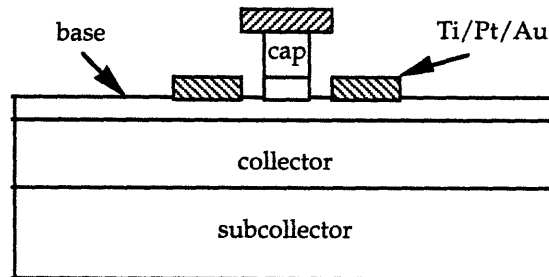
Figure 2.15: Schematic picture of a typical two-finger microwave HBT
© William Liu

The passivation ledge in a typical HBT, as shown in Figure 2.1, is the active emitter layer which extends as far as the base contacts. Normally, to contact the base, one must etch away this depleted AlInP layer to reach the p-type base layer. However, prior to indiscriminately etching all of this AlInP layer, a surface mask is used to protect a narrow depletion ledge which surrounds the emitter mesa and prevents it from being removed. Once the photoresist is defined to protect the not-to-be etched AlInP, a solution of $H_3PO_4 : HCl$ is used to etch down to the base surface.

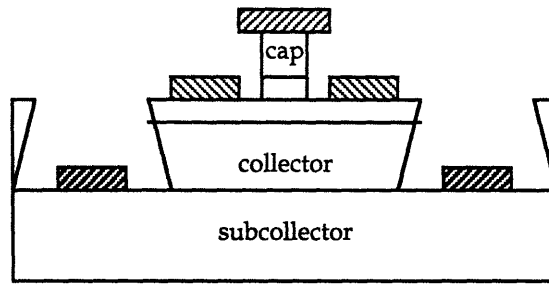
The process sequence for a microwave device is delineated in Figure 2.16. A description of each step is given in the caption following the illustration.



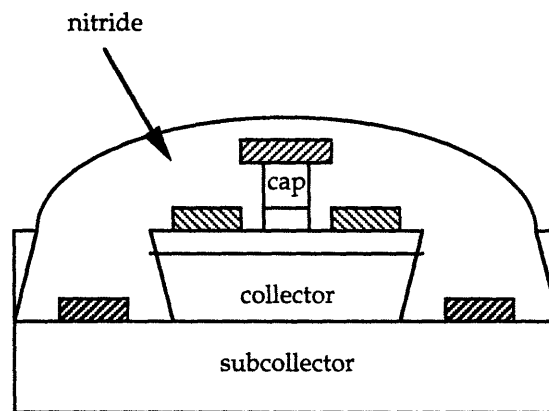
1. Use emitter mask to evaporate AuGe/Ni/Au emitter contacts.
Anneal at 430° C



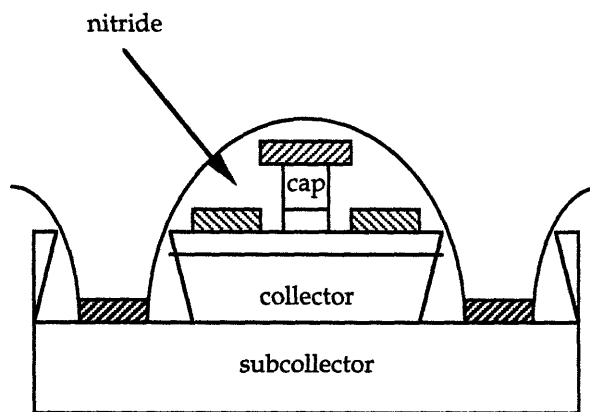
2. Etch down to base. Evaporate Ti/Pt/Au base contacts.



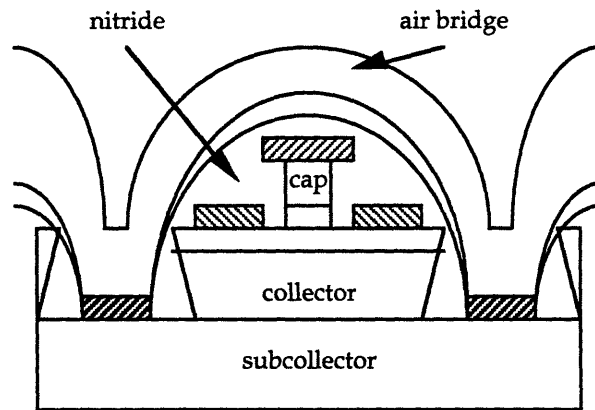
3. Use collector mask. Etch down to subcollector. Evaporate AuGe/Ni/Au collector contacts. Anneal contacts.



4. Deposit Nitride



5. Use photoresist and "Pads" mask to etch nitride around collector contacts



6. Evaporate Airbridge and liftoff resist.

Figure 2.16: R. F. processing sequence

2.3 Summary

Table 2.3 shows a summary of device fabrication, highlighting the differences in d. c. and r. f. process. The methods discussed in this chapter were used extensively in making the devices under investigation, the results of which are presented in the next section.

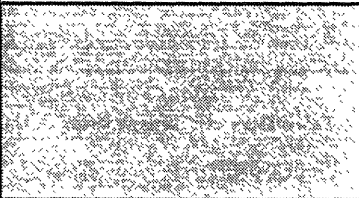
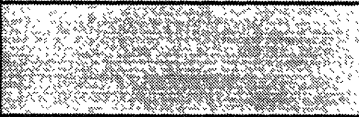
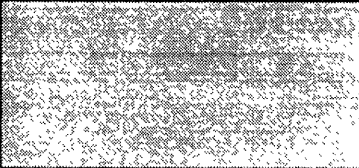
Layer	D. C. Process	R. F. Process
Emitter	solvent clean spin photoresist expose to "EMITTER" mask pattern develop, inspect bake clean developed surface evaporate AuGe/Ni/Au contacts liftoff	solvent clean spin photoresist expose to "EMITTER" mask pattern develop, inspect bake at 80° C, 3 minutes clean surface evaporate AuGe/Ni/Au contacts liftoff <i>Alloy contacts at 430° C</i>
Base	wet etch (H ₂ SO ₄ :H ₂ O ₂ :H ₂ O) to remove GaAs cap layer wet etch (H ₃ PO ₄ :HCl) to remove AlInP active emitter layer spin photoresist expose to "BASE" mask pattern develop, inspect clean surface evaporate Ti/Pt/Au contacts liftoff	use a combination of H ₂ SO ₄ :H ₂ O ₂ :H ₂ O and reactive ion etching (RIE) techniques to remove cap and emitter material spin photoresist expose to "BASE" mask pattern develop, inspect clean surface evaporate Ti/Pt/Au contacts liftoff
Collector	spin photoresist expose to "COLLECTOR" mask pattern develop, inspect clean surface evaporate AuGe/Ni/Au contacts liftoff Alloy contacts at 430° C [DONE]	spin photoresist expose to "COLLECTOR" mask pattern develop, inspect clean surface evaporate AuGe/Ni/Au contacts liftoff Alloy Contacts at 430° C
Pads		spin photoresist expose to "PAD" mask pattern develop, inspect bake at 80° C, 3 minutes clean surface evaporate Ti/Pt/Au pads liftoff, inspect
Airbridge I		spin photoresist expose to "AIRBRIDGE 1" mask pattern develop, inspect
Airbridge II		spin photoresist expose to "AIRBRIDGE 2" mask pattern develop, inspect plate surface with Au. [DONE]

Table 2.3: Summary of microwave and d. c. device fabrication

Chapter 3

Device Performance

This chapter describes the experimental results for the first reported Npn HBTs based on the AlInP material system. Three distinct devices; AlInP/GaAs, AlInP/GaInP, and AlInP/AlGaAs HBTs, were fabricated. Their performance results are discussed in the following sections. Chapter 4 presents a comparison of the AlInP material system with the better known material systems of GaInP and AlGaAs.

3.1 AlInP/GaAs Npn HBT

The epitaxial structure of this device is presented in Chapter 2. The d. c. characteristics of the fabricated HBTs were measured with a Semiconductor Parameter Analyzer and the current-voltage characteristics (I_C - V_{CE}) are shown in Figure 3.1.

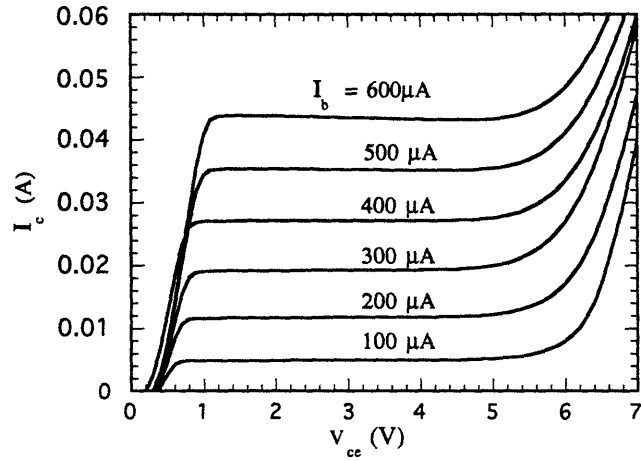


Figure 3.1 I_C - V_{CE} characteristics of an AlInP/GaAs Npn HBT

The common-emitter current gain of these devices is as high as 100 using an emitter area of $100 \times 100 \mu\text{m}^2$. The breakdown voltage, BV_{CEO} , is $\sim 6.5 \text{ V}$, consistent with the collector design used for this study. The offset voltage, $V_{ce(on)}$, is approximately 0.4 V , a value that is in good agreement with the measurement of the base-emitter and base-collector junction diode characteristics.

A Gummel plot of the same device is shown in Figure 3.2.

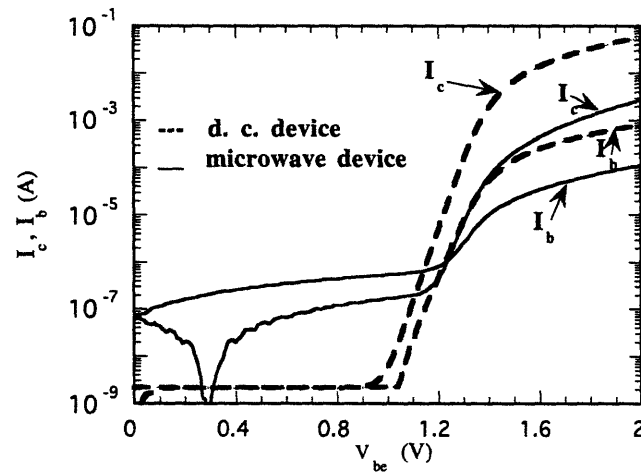


Figure 3.2 Gummel plot of a d. c. and microwave AlInP/GaAs HBT

The ideality factor, η_b , for the base current was measured at 1.48. The various components of base current have been presented in section 1.1.2.1. The surface recombination current is believed to be negligible for this device because of its large size. Therefore, the measured $\eta_b = 1.48$ indicates that the recombination currents in both the space-charge region and the base layer are equally important. For the collector current, η_c is 1.13. This ideality factor deviating from unity for the abrupt AlInP/GaAs base-emitter junction indicates a significant conduction-band discontinuity, ΔE_c , in the AlInP/GaAs heterojunction. It has been previously demonstrated in GaInP/GaAs HBTs that, if ΔE_c is small, the collector current is limited by the transport through the base layer and exhibits a unity ideality factor¹³. Figure 3.2 also shows a Gummel plot of a $2 \times 60 \mu\text{m}^2$ microwave device. Measured ideality factors for collector and base currents, respectively, are 1.38 and 2.52. The increase in η_b from d. c. to microwave device indicates that, because of the reduction in device size, the surface recombination currents both in the extrinsic base surface and implantation boundary are no longer negligible in the microwave transistor.

Figure 3.3 illustrates the measured current gain values of the two-finger microwave device having a total emitter area of $2 \times 60 \mu\text{m}^2$ and a device having an area of $100 \times 100 \mu\text{m}^2$.

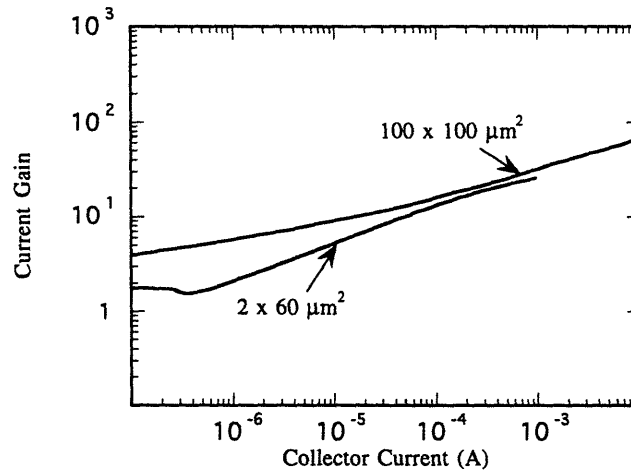


Figure 3.3: Measured current-gain values of a two-finger microwave device having a total emitter area of $2 \times 60 \mu\text{m}^2$ and a big device having an area of $100 \times 100 \mu\text{m}^2$.

¹³ "Current Transport Mechanism in GaInP/GaAs Heterojunction Bipolar Transistors," W. Liu, S. Fan, T. Kim, E. Beam, and D. Davito, *IEEE Transactions on Electron Devices*, vol. 40, no. 8, pp. 1378-1383, August 1993.

In general, the relationship between the current gain, β , and the emitter dimension (emitter width: W_E , emitter length: L_E) can be expressed as:

$$\frac{1}{\beta} = \frac{(J_{br} + J_{re})}{J_c} + 2 \frac{K_{surf}}{J_c} \cdot \left(\frac{1}{2W_E + 2L_E} \right)$$

where J_{br} (A/cm^2) and J_{re} (A/cm^2) are the base bulk recombination current density and the base-emitter space-charge region recombination current density, respectively, and K_{surf} (A/cm) is the surface recombination current divided by the emitter periphery.¹⁴ Because of the difference in their perimeter to area ratios, isolation implantation leakage current is larger in the r. f. device. Such high leakage current is also evident in Figure 3.2, which shows that at $V_{be} \leq 1.2$ V, the base leakage current remains relatively constant at $0.1 \mu A$. The highest current gain values are 100 and 20 for the d c. and microwave devices, respectively.

Figure 3.4 illustrates the high-frequency performance of the $2 \times 60 \mu m^2$ device in the common-emitter configuration.

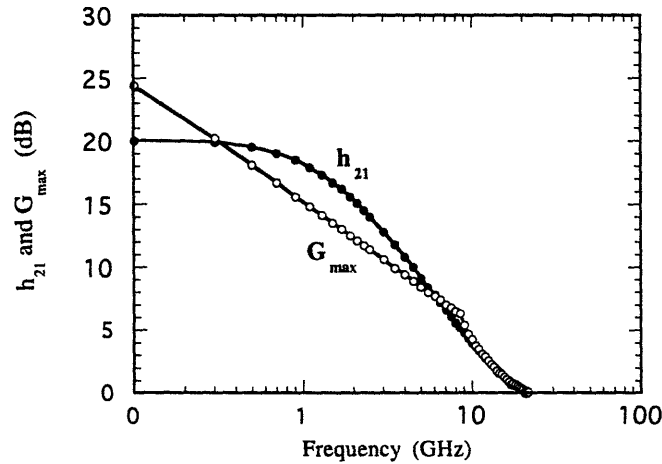


Figure 3.4: High-frequency performance of the $2 \times 60 \mu m^2$ AllnP/GaAs device in the common-emitter configuration

Cutoff frequency, f_T , is defined as the frequency at which the magnitude of the common-emitter current gain, h_{21} , drops to unity. Quantitatively, this frequency is:

¹⁴ "Extrinsic Base Surface Recombination Current in GaInP/GaAs Heterojunction Bipolar Transistors with Near-Unity Ideality Factor," W. Liu, *Jpn. J. Appl. Phys.*, vol 32 (1993) pp. L713-L715), May, 1993.

$$f_T \approx \frac{1}{2\pi\tau_{\text{eff}}}$$

where τ_{eff} is the effective delay time:

$$\tau_{\text{eff}} = \tau_e + \tau_c + \tau_b + \tau_{\text{cr}}$$

τ_e , in turn, is the emitter charging delay, τ_b is the base transit delay, τ_c is the collector transit delay, and τ_{cr} is the collector charging delay.

The maximum oscillation frequency, f_{max} , is a measure of power gain. It is the frequency at which maximum available power gain, G_{max} , of the transistor falls off to unity and is expressed as:

$$f_{\text{max}} = \sqrt{\frac{f_T}{8\pi R_b C_{bc}}}$$

where f_T is the cutoff frequency, R_b is the base resistance, and C_{bc} is the total base-collector capacitance of the device. These two parameters, f_T and f_{max} , presented here in simplified form, indicate frequency ranges in which the transistor operation is stable. For the measurements reported here, the AlInP/GaAs device was operated at a collector current of 48 mA, and the collector-emitter bias was 6 V. The cutoff frequency, f_T , is measured at 20 GHz. The maximum oscillation frequency (f_{max}) is 24.4 GHz. These results are believed to be the first reported values of HBTs based on the AlInP/GaAs material system. The base contact resistance and base sheet resistance measured from a transmission line pattern are $2.3 \times 10^{-3} \Omega \cdot \text{cm}^2$ and $620 \Omega/\text{sq}$, respectively. It is believed that the base doping level ($1 \times 10^{19} \text{ cm}^{-3}$) used is only moderate. As can be seen from the equation defining f_{max} , increased base doping reduces base resistance, thereby increasing f_{max} . Therefore, significantly improved performance is expected when a higher doping level is chosen.

In summary, the first known d. c. and microwave performance results of Npn AlInP/GaAs HBTs have been reported. The next section gives results obtained from AlInP/GaInP and AlInP/AlGaAs transistors.

3.2 AlInP/GaInP and AlInP/AlGaAs HBTs

The structure and doping levels for the AlInP/GaInP HBT are discussed in Chapter 2. For the AlInP/AlGaAs HBT, however, the base-collector junction is also a heterojunction. The

epitaxial structure for this device consists of a 2000 Å n⁺ GaAs cap layer doped at 5 × 10¹⁸ cm⁻³, a 1000 Å n AlInP active emitter layer doped at 5 × 10¹⁷ cm⁻³, a 1000 Å p⁺ AlGaAs base layer doped at 1 × 10¹⁹ cm⁻³, a 5000 Å n⁻ GaAs collector layer doped at 2 × 10¹⁶ cm⁻³, and an 1 μm n⁺ GaAs subcollector doped at 3 × 10¹⁸ cm⁻³. The AlGaAs base material and GaAs collector material create a heterojunction at the base-collector interface of the device. The resulting energy band model is given schematically in Figure 3.5.

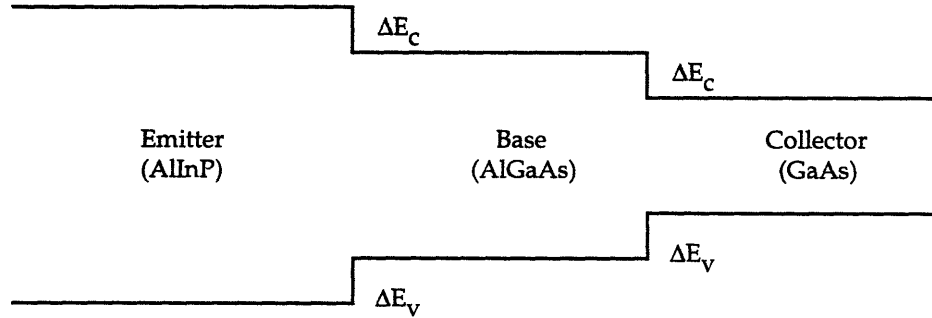
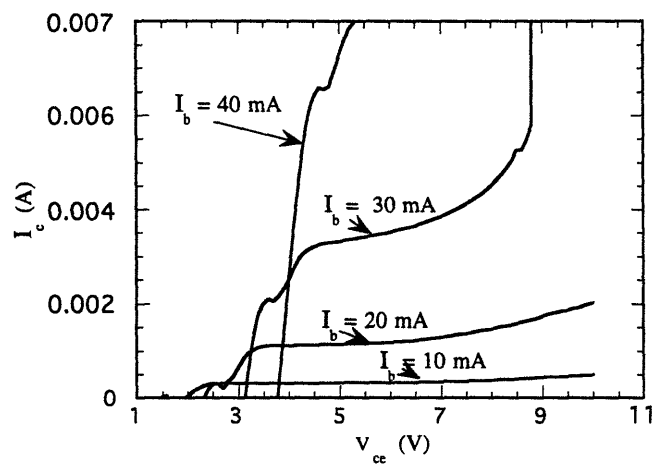


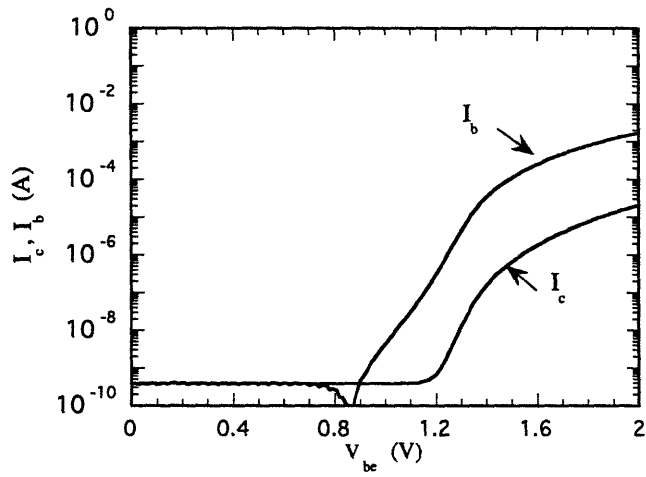
Figure 3.5: Simplified energy-band diagram for an AlInP/AlGaAs/GaAs HBT emphasizing the heterojunction at the base-collector interface

Because of a conduction band discontinuity, ΔE_c , at the base-collector junction, electrons injected from the base into the collector acquire kinetic energy through the potential step. As a result, these carriers travel through the collector in a smaller amount of time, thereby reducing τ_c , the collector transit time. AlGaAs was not used as collector material because its electron saturation velocity is less than that of GaAs. Therefore, transit time across an AlGaAs collector would be far greater than the collector transit time of GaAs material.

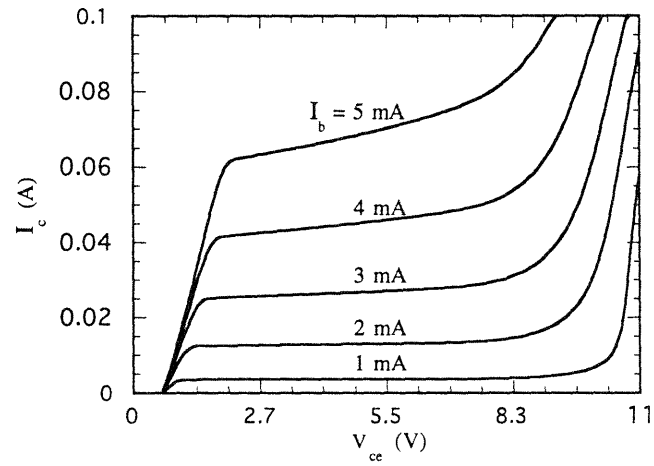
The fabrication of AlInP/GaInP and AlInP/AlGaAs HBTs yielded poor performance results from these devices. The d. c. current-voltage characteristics of these HBTs as well as their respective Gummel plots are shown in Figure 3.6.



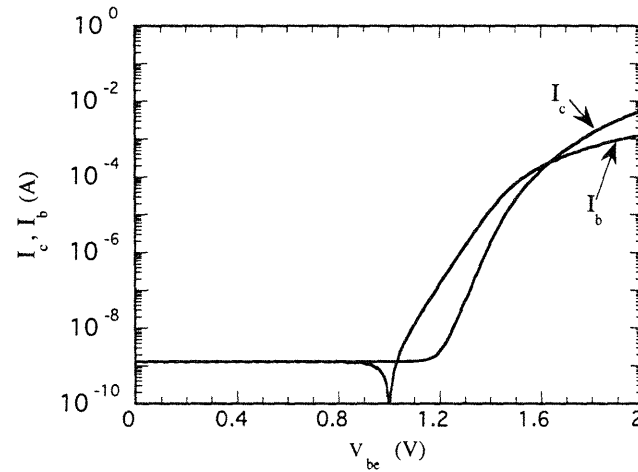
(a) I_c - V_{ce} characteristics of a $100 \times 100 \mu\text{m}^2$ AlInP/GaInP Npn HBT



(b) Gummel plot of a $100 \times 100 \mu\text{m}^2$ AlInP/GaInP Npn HBT



(c) I_c - V_{ce} characteristics of a $100 \times 100 \mu\text{m}^2$ AlInP/AlGaAs Npn HBT



(d) Gummel plot of a $100 \times 100 \mu\text{m}^2$ AlInP/AlGaAs Npn HBT

Figure 3.6: I_c - V_{ce} characteristics and Gummel plots of the processed AlInP/GaInP (a, b) and AlInP/AlGaAs (c, d) transistors

Note the high I_b and V_{ce} bias used in both of these devices in order to obtain transistor performance in the forward-active region ($\beta > 1$). The common-emitter current gain of the

AlInP/AlGaAs device is 4. The breakdown voltage is ~ 10.3 V, and $V_{ce(on)}$, is ~ 0.7 V. For the AlInP/GaInP HBT, a current gain of 2, BV_{ceo} of 11.0 V, and a $V_{ce(on)}$ of 2.0 V was measured.

Measurement of current ideality factors of these devices reveals high η_b and η_c for both HBTs. Specifically, the ideality factor for I_b of the AlInP/GaInP device is 1.52 and for the collector current, $\eta_c = 1.16$. Similarly, for the AlInP/AlGaAs device, $\eta_b = 1.69$ and $\eta_c = 1.15$. Such high η_c values, in particular, indicate a severe conduction band discontinuity in the emitter-base heterojunction. As a result, the nonoptimized fabrication of these devices is possibly due, in part, to a staggered-band lineup at the AlInP/GaInP and AlInP/AlGaAs interfaces. Preliminary studies have been conducted on the staggered band line up of InGaP/AlGaAs heterojunctions¹⁵. In a typical HBT, the heterojunction band diagram is as shown in Figure 3.7. In a staggered line-up, the heterointerface band line up is as illustrated in Figure 3.8.

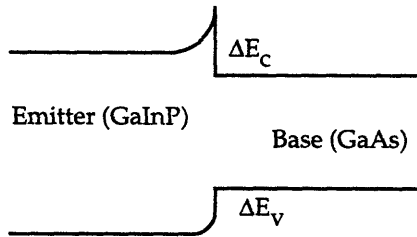


Figure 3.7: Emitter-base band diagram in a typical HBT

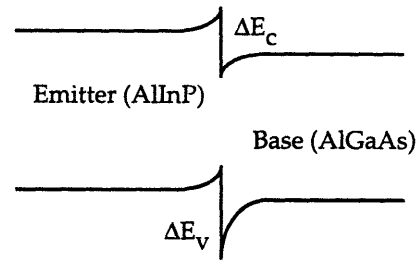


Figure 3.8: Staggered band diagram at the emitter-base junction of an HBT

More investigation of the band discontinuities of AlInP based systems is necessary before a conclusion on band structures of these devices can be reached. Nevertheless, in a junction band configuration with severe discontinuities, the line-up prevents electrons from easily traversing the emitter-base junction, thereby reducing emitter current across this interface. As the height of the potential barrier between the emitter-base regions is controlled by the emitter-base voltage, V_{be} , a large forward bias of this junction reduces the barrier height, thereby enabling carriers to cross this interface. This effect is seen in the current-voltage diagrams of these devices. High values of $V_{ce(on)}$ for these two transistors show that the junction barrier for AlInP/AlGaAs and AlInP/GaInP devices are not ideal for desired transistor performance. The high values of I_b used in this forward-active region of operation also indicate that a significant

¹⁵ "Observation of staggered band lineup in $In_{0.5}Ga_{0.5}P/Al_{0.43}Ga_{0.57}As$ heterojunction grown by liquid phase epitaxy," J. B. Lee, K. Kim, and B. Choe, *Appl. Phys. Lett.*, 62 (21), May 1993, pp. 2688-2690.

amount of base current is lost due to recombination, probably in the space-charge region of the junction.

The nonoptimal performance of the AlInP/AlGaAs and AlInP/GaInP HBTs is believed to be due primarily to short minority carrier lifetimes in the base region of these transistors. Nonetheless, a severe conduction-band discontinuity at the emitter-base interface is evident from both current-voltage plots and ideality factors. A high temperature performance experiment has been conducted on these devices to investigate the effects on current gain and, consequently, device performance. The results are presented in section 4.3. For AlInP/GaAs HBTs, the conduction band discontinuity is not severe enough to significantly disrupt transistor performance, thereby enabling measurement of preliminary high-frequency performance of these devices. For AlInP/GaAs HBTs, an f_T of 20 GHz and an f_{max} of 24.4 GHz were obtained.

Chapter 4

Comparison of Different Material Systems

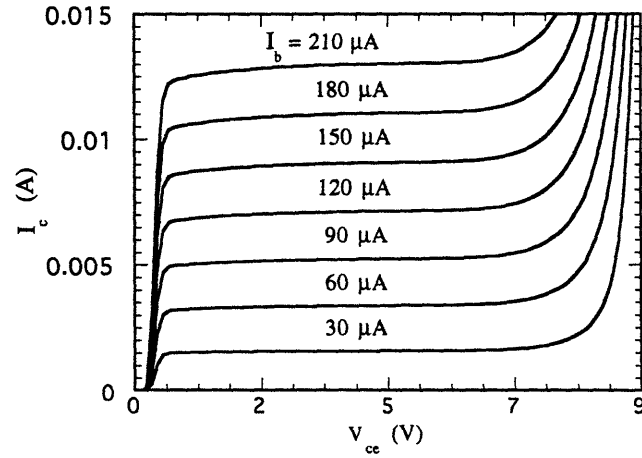
Two additional HBTs; AlGaAs/GaAs and GaInP/GaAs, were also processed for this investigation in an effort to compare the transistor performance of the AlInP material system with the better known material systems of GaInP and AlGaAs. Identical structures, doping densities, and fabrication methods were implemented in these two devices. This information has been presented in Chapter 2. Two additional experiments: passivation and high temperature measurements, were also conducted on AlInP/GaAs HBTs. These results are discussed in the context of previously published performance of GaInP/GaAs and AlGaAs/GaAs HBTs.

4.1 GaInP/GaAs and AlGaAs/GaAs HBTs

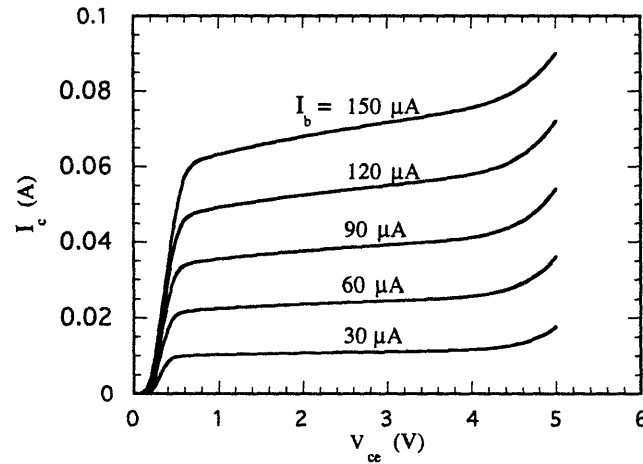
The fabricated GaInP/GaAs and AlGaAs/GaAs HBTs used for this investigation yielded typical performance results for these types of devices.^{16,17} The d. c. current-voltage characteristics of these devices are shown in Figure 4.1.

¹⁶ *Microwave and D.C. Studies of Npn and Pnp AlGaAs/GaAs Heterojunction Bipolar Transistors*, W. Liu, Ph.D. Dissertation, Stanford University, Stanford, CA, February 1991, p. 126.

¹⁷ "Near-Ideal I-V Characteristics of GaInP/GaAs Heterojunction Bipolar Transistors," W.Liu, and S. Fan, *IEEE Electron Device Letters*, vol. 13, no. 10, October 1992.



(a) I_c - V_{ce} characteristics of a $100 \times 100 \mu\text{m}^2$ AlGaAs/GaAs HBT

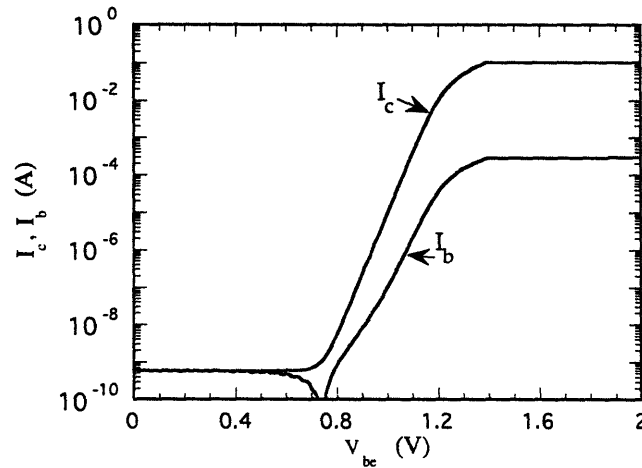


(b) I_c - V_{ce} characteristics of a $100 \times 100 \mu\text{m}^2$ GaInP/GaAs HBT

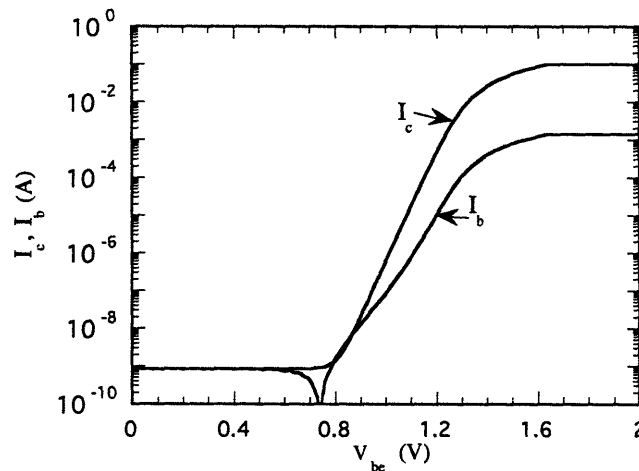
Figure 4.1: I_c - V_{ce} plots of (a) AlGaAs/GaAs and (b) GaInP/GaAs HBTs

The current gain, β , of the GaInP/GaAs device is approximately 440. β for the AlGaAs/GaAs transistor is 70. BV_{ce0} for GaInP/GaAs HBT is ~ 5.0 V. $V_{ce(on)}$ is 0.35 V. For the AlGaAs/GaAs device, BV_{ce0} is measured at ~ 8.0 V and $V_{ce(on)}$ is 0.3 V. These $V_{ce(on)}$ values in particular are the lowest turn-on voltages of the five transistors which were processed for this thesis. Since a turn-on voltage as close to zero volts as possible is ideal, these values are more desirable for good transistor performance than the higher values reported for the AlInP HBTs.

The Gummel plot of the GaInP device, shown in Figure 4.2 (a), yields ideality factors of 1.04 and 1.30 for collector and base currents, respectively. As measured from Figure 4.2 (b), ideality factors for the AlGaAs/GaAs device are 1.07 and 1.49 for collector and base currents, respectively.



(a) Gummel plot of a $100 \times 100 \mu\text{m}^2$ GaInP/GaAs HBT



(b) Gummel plot of an AlGaAs/GaAs HBT

Figure 4.2: (a) Gummel plot of GaInP/GaAs HBT and
(b) Gummel plot of an AlGaAs/GaAs HBT

Note that η_c values are close to unity for both types of devices. Particularly when compared to AlInP/GaInP and AlInP/AlGaAs HBTs, these numbers suggest that AlGaAs/GaAs and GaInP/GaAs HBTs have a much better band line-up; i.e. smaller conduction-band discontinuity at the heterointerface between emitter and base junctions.

A comparison of current gain values of the five fabricated devices is presented in Figure 4.3.

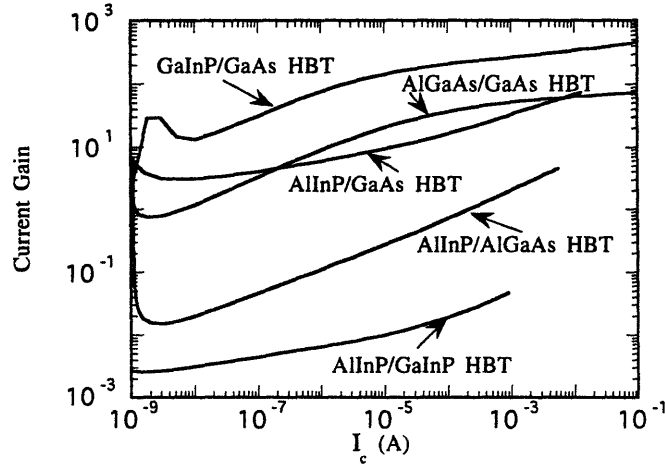


Figure 4.3: Current gains of all devices: AlInP/GaAs, AlInP/AlGaAs, AlInP/GaInP, GaInP/GaAs, and AlGaAs/GaAs HBTs processed for this investigation

As can be seen from Figure 4.3, the most favorable transistor performance achieved within the AlInP material system is with the HBT having an AlInP/GaAs emitter-base. Its performance level is comparable to AlGaAs/GaAs HBTs but still falls short of GaInP/GaAs device current gain. AlInP/GaInP and AlInP/AlGaAs devices yield disappointing performance levels. Table 4.1 summarizes the measured transistor parameters of all devices fabricated for this thesis.

HBT E/B/C	β	$V_{ce(on)}$ (V)	BV_{ceo} (V)	η_c	η_b
AlInP/GaAs/GaAs	100	0.40	6.5	1.13	1.48
AlInP/AlGaAs/GaAs	4	0.70	10.3	1.15	1.69
AlInP/GaInP/GaInP	2	2.00	11.0	1.16	1.52
GaInP/GaAs/GaAs	440	0.35	5.0	1.04	1.30
AlGaAs/GaAs/GaAs	70	0.30	8.0	1.07	1.49

Table 4.1: Transistor parameters measured from the devices fabricated for this investigation

4.2 Passivation

Since a free GaAs surface is characterized by a high surface recombination velocity, surface recombination significantly degrades $1/f$ noise performance in unpassivated HBTs. Surface passivation has previously been demonstrated in AlGaAs/GaAs and GaInP/GaAs HBTs¹⁸. This section presents initial results on the passivation of AlInP/GaAs devices.

In this investigation, both passivated and unpassivated AlInP/GaAs HBTs, having an emitter area as small as $4 \times 20 \mu\text{m}^2$, were fabricated and compared. Passivation experiments were not performed on AlInP/GaInP or AlInP/AlGaAs HBTs due to the low β values obtained for these devices. A peak current gain of 150 was measured for the passivated AlInP/GaAs devices. Unpassivated devices yielded current gains of 100.

Passivated devices with various emitter widths and ledge widths were fabricated. The distance between the edge of the depletion ledge to the base metal was $\sim 3 \mu\text{m}$. Figure 4.4 illustrates measured Gummel plots of $4 \times 20 \mu\text{m}^2$ devices with ledge width, W_L , of $1 \mu\text{m}$ (passivated) and ledge width of 0 (unpassivated).

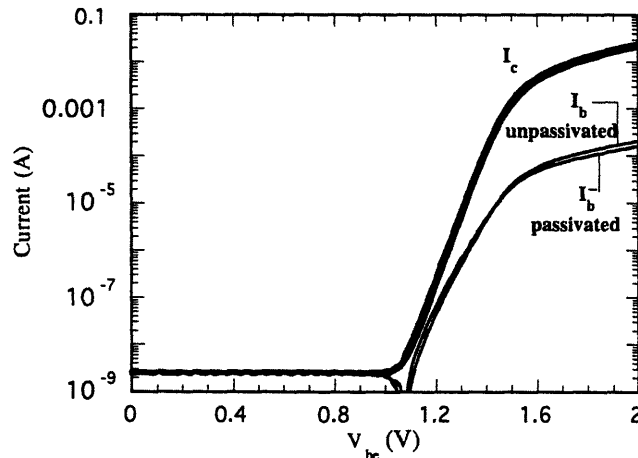
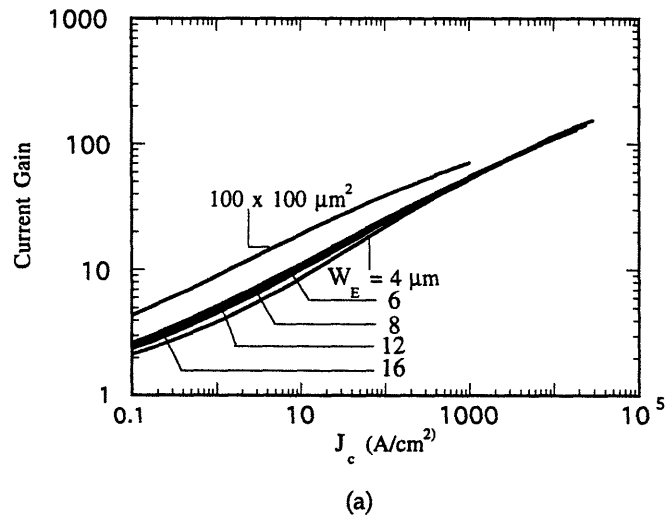


Figure 4.4: Gummel plot of a passivated $4 \times 20 \mu\text{m}^2$ AlInP/GaAs device

¹⁸ "Extrinsic Base Surface Passivation in GaInP/GaAs Heterojunction Bipolar Transistors," W. Liu, E. Beam, T. Henderson, and S. Fan, *IEEE Electron Device Letters*, vol. 14, no. 6, June, 1993.

As can be seen from Figure 4.4, the collector currents are almost identical whereas the base current decreases slightly for passivated devices. Unlike passivated GaInP/GaAs HBTs which show a dramatic reduction in I_b and, therefore, a significant increase in β , the results obtained here for AlInP/GaAs devices indicate only a 1.5 to 2-fold increase in passivated current gain. In general, base current components such as base bulk recombination current and base-emitter space-charge recombination current are proportional to the emitter area. The extrinsic base surface recombination current, in contrast, is proportional to the length of the emitter periphery. Therefore, in unpassivated devices where the extrinsic base surface recombination current is significant, the current gain decreases as emitter area decreases. A quantitative description of current gain with respect to emitter dimensions is given in section 3.1. Figure 4.5 (a) shows that for an AlInP/GaAs HBT, the measured β for an unpassivated $100 \times 100 \mu\text{m}^2$ device, which has negligible surface recombination due to its large emitter area, exhibits higher current gain than the β of smaller, passivated, devices. A comparison with current gains of unpassivated devices of the same small dimensions (Figure 4.5 (b)) indicates that the ledge thickness used in this experiment ($\sim 1000 \text{ \AA}$) may not be completely depleted since the two graphs are almost identical, suggesting improper passivation of devices.



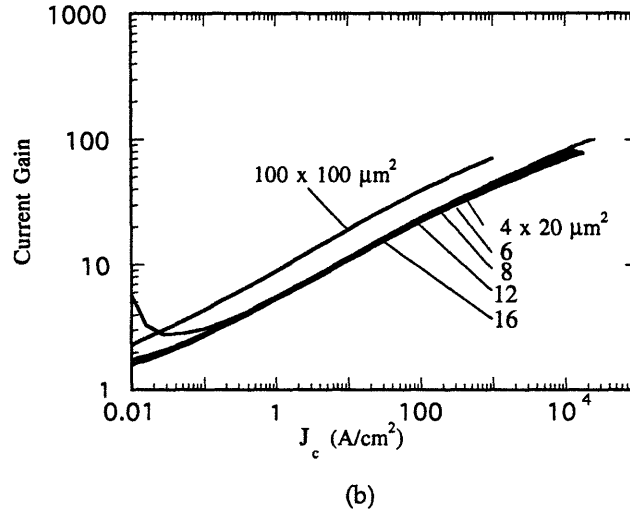


Figure 4.5: Current gain versus collector current density for an (a) passivated and (b) unpassivated AlInP/GaAs device

The depletion layer width, d , can be approximated from the following equation:

$$d = \sqrt{\frac{2\epsilon_s V_o}{q N_{ne}}}$$

where ϵ_s is the dielectric permittivity of the material, q is electronic charge, and V_o is the potential drop across the barrier. Using this approximation, the air depletion width of the ledge is estimated at $\sim 490 \text{ \AA}$ for a typical HBT (using AlGaAs emitter material). The depletion width at the emitter-base junction is estimated to be $\sim 130 \text{ \AA}$. Given these calculations, it is possible that approximately 380 \AA of the AlInP ledge may not be depleted. For more specific computations, the permittivity of AlInP should be determined. Given the likelihood of an undepleted ledge, however, when the emitter-base junction is forward biased, the junction depletion region decreases and parasitic emitter current first flows through the undepleted portion of the passivation ledge and then, upon reaching the end of the ledge near base contacts, is injected into the base. Because this current is injected closer to the base contact, it increases base contact recombination current.

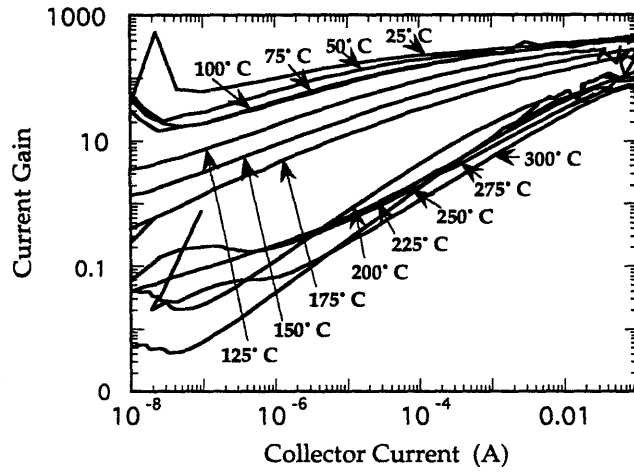
Another possible reason for poor passivation is that base bulk and space-charge region recombination currents may dominate over the surface recombination component of I_b for AlInP material. AlInP has significantly more recombination centers associated with oxygen complexes, which are often incorporated when aluminum is used in the emitter epitaxial

growth. Therefore, the elimination of I_{surf} does not result in substantial increase in the current gain of these devices. The approximate trap density of AlInP was measured using deep level transient spectroscopy.¹⁹ The results confirm that AlInP has significantly more recombination centers than its GaInP counterpart. Further analysis of material characteristics and a separate investigation of optimal ledge thickness of AlInP is required for proper passivation of these devices.

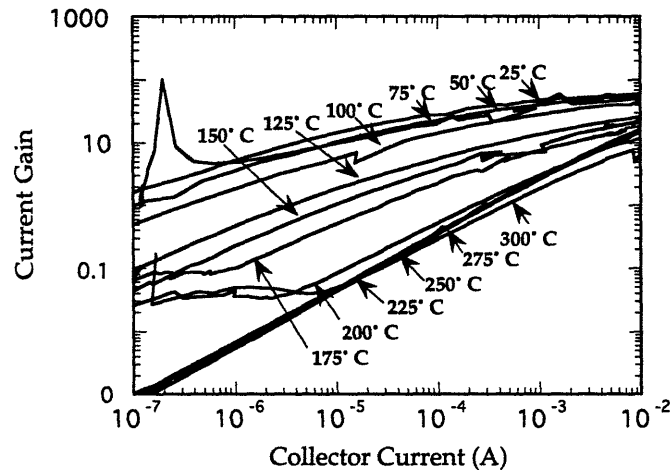
4.3 Temperature Dependence of Current Gain in AlInP/GaAs, AlInP/GaInP, and AlInP/AlGaAs HBTs

This section presents the results from a study of temperature dependence of current gains of the AlInP/GaAs, AlInP/GaInP, and AlInP/AlGaAs HBTs fabricated for this thesis. In this investigation, the current gains of the AlInP HBTs operated at temperatures between 25° C and 300° C were measured. The base-collector bias was maintained at 0 V such that the actual junction temperature could be approximated as the externally applied substrate temperature. These measurements indicate that the current gain increases for all AlInP devices tested under increasing temperature conditions. The GaInP/GaAs and AlGaAs/GaAs HBTs were also measured for comparison (Figure 4.6).

¹⁹ Measurements conducted by Tae Kim, a member of technical staff at Texas Instruments, Inc.



(a)

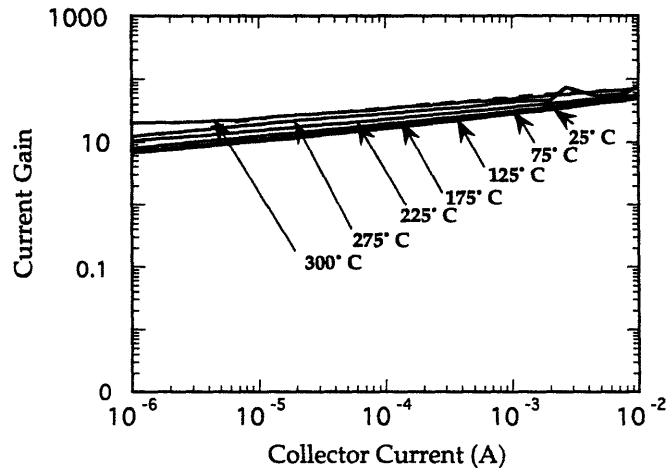


(b)

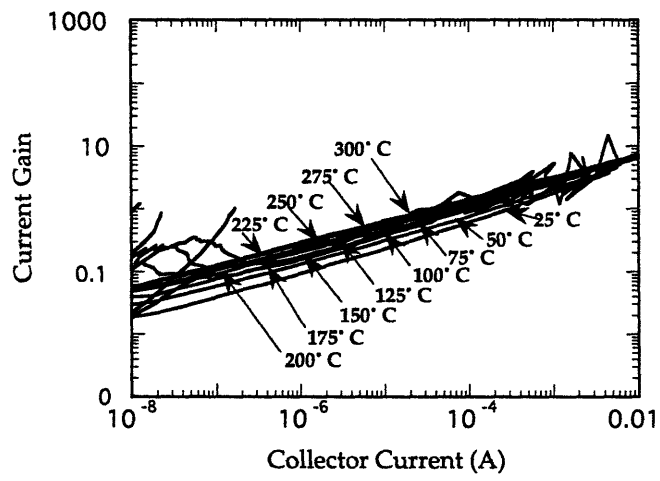
Figure 4.6: Temperature dependence of current gain in (a) GaInP/GaAs and (b) AlGaAs/GaAs HBTs

For both of these devices, current gain decreased substantially with increasing temperature.

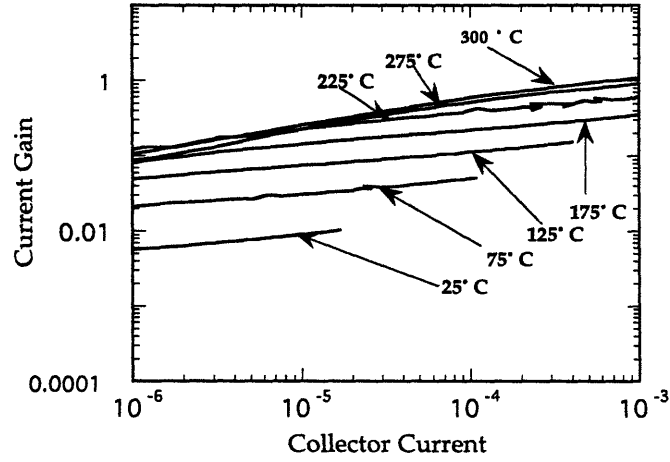
Figure 4.7 presents current gain versus collector current at different substrate temperatures for the AlInP HBTs under study. As can be seen from these measurements, β increases with an increase in temperature.



(a)



(b)



(c)

Figure 4.7: Temperature dependence of current gain in (a) AllnP/GaAs, (b) AllnP/AlGaAs, and (c) AllnP/GaInP HBTs

In general, current gain in HBTs is limited either by lifetime of minority carriers in the base or by back-injection of holes at the emitter-base junction. The latter case is quantitatively described by the emitter injection efficiency which, as defined in Chapter 1, is:

$$\gamma = \frac{I_{ne}}{I_{ne} + I_{pe}} \approx \frac{D_{nb} N_{ne} L_{pe} n_{ib}^2}{D_{nb} N_{ne} L_{pe} n_{ib}^2 + D_{pe} N_{pb} W_b n_{ie}^2}$$

For a more quantitative analysis of minority carrier lifetime in the base, the base transport factor, α , is used. α is defined as the ratio of the current diffusing into the collector to the current injected at the emitter-base junction and is expressed as:

$$\alpha = \frac{I_{nc}}{I_{ne}} \approx 1 - \frac{W_b^2}{2L_{nb}^2} = 1 - \frac{W_b^2}{2D_{nb}\tau_{nb}}$$

Essentially, this factor measures the number of carriers that traverse the device from emitter to collector without recombining in the base. Given these definitions, β can now be restated as:

$$\beta = \frac{\alpha\gamma}{1 - \alpha\gamma}$$

For non-ideal devices, both α and γ are less than unity, and the extent to which they depart from unity represents a hole current that must be supplied from the base contact. Whichever variable deviates the most from unity dominates as the factor that limits the current gain of the transistor. If it is assumed that back-injection of holes from the base to emitter is negligible due to a severe junction barrier faced by these carriers, then $\gamma \rightarrow 1$ and β is approximated as $\frac{\alpha}{1 - \alpha}$. Therefore, current gain is limited by transport of carriers across the base layer. Conversely, if back-injected holes is higher in comparison to recombination of carriers in the base region, i. e. $\alpha > \gamma$, for a first approximation, $\alpha \rightarrow 1$, and the back-injected current at the emitter-base junction becomes the limiting factor of current gain.

The temperature dependence of β helps determine the dominant factor that limits the current gain of a transistor. If β decreases as temperature increases, γ dominates as limiting factor of current gain and an increase in temperature causes an increase in the back-injection of holes by increasing the kinetic energy of these carriers. As a result, more of these holes overcome the junction barrier, increasing I_b and, consequently, decreasing β . This is the case for the measured GaInP/GaAs and AlGaAs/GaAs transistors in this investigation.

For all of the AlInP HBTs, however, current gain increases with temperature for the same range of temperatures. This trend suggests that β for these devices is limited by minority carrier transport through the base. Therefore:

$$\beta = \frac{\alpha}{1 - \alpha} \approx \frac{2L_{nb}^2}{W_b^2} = \frac{2D_{nb}\tau_{nb}}{W_b^2}$$

W_b and τ_{nb} are relatively insensitive to temperature. D_{nb} , however, is a function of temperature:

$$qD_{nb} = \mu_n kT$$

where μ_n is the electron mobility, k is Boltzman constant, and T is temperature. If one assumes, for a first approximation, that μ_n changes very little for a given temperature range, it can be seen that the diffusion coefficient increases with temperature. An increase in D_{nb} results in an increase in L_{nb} , which, in turn, results in an increase in β . In effect, as temperature increases, current gain increases. This effect is seen in the temperature measurements of the AlInP HBTs under investigation. At even higher temperatures, however, it is speculated that these devices would behave similar to their GaInP and AlGaAs counterparts, and a decrease in current gain would result as temperature is increased since back-injected holes would become a significant factor of base current.

Conclusions

This thesis has presented fabrication and performance results for the first reported Npn HBTs based on the AlInP material system. Three devices were processed: AlInP/GaAs, AlInP/AlGaAs, and AlInP/GaInP HBTs. The highest current gains of 100 were achieved with the AlInP/GaAs HBT. This device was also processed for high frequency testing. The cutoff frequency and the maximum oscillation frequency were measured at 20 GHz and 24.4 GHz, respectively. These results are believed to be the first reported values of HBTs based on the AlInP/GaAs material system.

In addition, preliminary passivation experiments were conducted on the AlInP/GaAs devices, yielding unsatisfactory results. Current gains increased only by $\sim 30\%$, in comparison to 80% and higher increases in previously reported results on GaInP based material. This small increase is attributed to a partially undepleted AlInP ledge.

Finally, high temperature measurements of AlInP based HBTs reveal an increase in current gain with temperature. These results suggest that the current gain of these devices is limited primarily by the transport of minority carriers across the base region.

GaInP/GaAs and AlGaAs/GaAs HBTs were also fabricated using identical doping densities and layer thicknesses in order to compare device performance between different material systems. Although AlInP/GaAs HBTs are comparable to their AlGaAs/GaAs counterparts, the AlInP/AlGaAs and AlInP/GaInP devices yielded very poor current gain values. Further analysis of material characteristics, band discontinuities, carrier lifetimes, and optimal passivation ledge thicknesses are warranted to improve device performance based on this material system.

References

- D. Hill, *Pnp Heterojunction Bipolar Transistors in AlGaAs/InGaAs/GaAs*, Ph.D. Dissertation, Stanford University, Stanford, CA, 1990.
- Juntao Hu, and D. Pavlidis, "Fabrication of GaInP/GaAs Heterojunction Bipolar Transistors," Prepared for :Epitaxial Products, Ltd., Wales, U. K. pp 1-10.
- H. Kawai, T. Kobayashi, F. Nakamura, and K. Taira, "Npn and Pnp GaInP/GaAs Heterojunction Bipolar Transistors Grown by MOCVD," *Electronics Letters*, vol. 25, iss. 9, pp. 609-610.
- A. Kikuchi, K. Kishino, and Yawara Kaneko, "High-optical-quality GaInP and GaInP/AlInP double heterostructure lasers grown on GaAs substrates by gas-source molecular-beam epitaxy," *J. Appl. Phys.* 66 (9), November 1989, pp.4557-4559.
- T. Kobayashi, K. Taira, F. Nakamura, and H. Kawai, "Band lineup for a GaInP/GaAs heterojunction measured by a high-gain Npn heterojunction bipolar transistor grown by metalorganic chemical vapor deposition," *J. Appl. Phys.* 65 (12), June 1989, pp.4898-4902.
- W. Liu, *Microwave and D. C. Studies of Npn and Pnp AlGaAs/GaAs Heterojunction Bipolar Transistors*, Ph.D. Dissertation, Stanford University, Stanford, CA, 1991.
- W. Liu, S. Fan, T. Henderson, and D. Davito, "Temperature Dependences of Current Gains in GaInP/GaAs and AlGaAs/GaAs Heterojunction Bipolar Transistors," *IEEE Transactions on Electron Devices*, vol. 40, no. 7, July 1993, pp.1351-1353.
- W. Liu and J. Harris, "Parasitic Conduction Current In the Passivation Ledge of AlGaAs/GaAs Heterojunction Bipolar Transistors," *Solid-State Electronics*, vol. 35, no. 7, 1992, pp. 891-895.
- J. Mayer, and S. Lau, *Electronic Materials Science for Integrated Circuits in Si and GaAs*. MacMillan Publishing Co, NY, 1990.

- G. Neudeck. *Modular Series on Solid State Devices;: The PN Junction Diode* , vol. 2, Addison-Wesley, MA, 1989.
- G. Neudeck. *Modular Series on Solid State Devices;: The Bipolar Junction Transistor.* vol. 3, Addison-Wesley, MA, 1989.
- R. Pierret, *Modular Series on Solid State Devices;: Semiconductor Fundamentals.* vol. 1, Addison-Wesley, MA, 1989.
- R. Pritchard, *Electrical Characteristics of Transistors*, McGraw-Hill Book Co., NY, 1967.
- M. Shur, *Physics of Semiconductor Devices*, Prentice Hall, NJ, 1990.
- S. M. Sze, *Physics of Semiconductor Devices*. New York: Wiley, 1981.
- M. Watanabe, J. Yoshida, M. Mashita, T. Nakanisi, and A. Hojo, "Band discontinuity for GaAs/AlGaAs heterojunction determined by C-V profiling technique," *J. Appl. Phys.* 57 (12), June, 1985, pp.5340-5344.